CHAPTER 1

Progenitor search in SN 1006

1.1. Introduction

The search for a donor star in SN 1572 has not turned up an obvious candidate. However, we have detected two objects (Tycho-B and Tycho-G) exhibiting some unusual properties, which while interesting, ultimately seem inconsistent with the expectations of any viable donor star scenario. Donor star scenarios are theoretical in their nature and any actual donor star is likely to not exhibit all features predicted by the model. Therefore, we have reached an impasse with SN 1572 and more detailed observations will likely not provide a definitive answer if either of these two stars were involved in the progenitor system. An obvious way forward is to scrutinise stars in other Type Ia supernova (SN Ia) remnants and see if any of those have similar properties to Tycho-B or Tycho-G. The remnant of SN 1006 is the ideal object for this kind of follow-up search.

The lack of a central neutron star, observation of several tenths of a solar mass of iron inside the remnant (Hamilton et al., 1997) and the the high peak luminosity and basic light curve shape (visible for several years Goldstein & Peng Yoke, 1965) all indicate that SN 1006 was a SN Ia. The remnant has a secure distance, measured by Winkler et al. (2003), who combined the proper motion and the radial velocity of the expanding shell to measure the distance to 2.2 kpc, making SN 1006 the closest of the ancient SN Ia remnants (consistent SN 1006 being the brightest). The geometric centre of the remnant is well determined from both X-ray and radio observations (Winkler et al., 2003). The interior of the remnant has been probed with UV background sources (Winkler et al., 2005). This revealed the aforementioned iron core as well as a silicon rich shell. The remnant has been searched for possible objects associated with the supernova explosion previously, and an unusual O-star had been identified as a possible donor star to SN 1006.

This unusual O-Star was identified near the centre of SN 1006 by Schweizer & Middleditch (1980) and is now called Schweizer-Middleditch Star (SM-Star). After successful identifications of neutron stars in both the Vela Remnant and the Crab Remnant this was thought to be the third identification of a stellar remnant in a historical supernova. Subsequent UV spectroscopic follow-up of the SM-Star by Wu et al. (1983), showed strong Fe II lines with a profile broadened by a few thousand km s^{-1}. In addition, Wu et al. (1983) identified redshifted Si II, Si III and Si IV lines. Their conclusion was that these absorption lines stem from the remnant and place the SM-Star behind the remnant, making it unre-

lated to SN 1006. Although unrelated, the SM-Star is an ideal object to probe the remnant and measure upper limits for interstellar extinction (E(B-V) = 0.1 Wu et al., 1993; Winkler et al., 2003).

SN 1006 has several properties which make it well suited to undertake a progenitor search. Although the remnant is the oldest among the known SN Ia remnants, its age is still young enough that the remnant's centre is well determined, and the motion of any potential donor star low enough that only a small area of stars need to be searched. Furthermore, this elapse of 1005 years is a short length of time relative to the timescales of stellar evolution for donor stars (see Marietta et al., 2000) - we still expect a potential donor star to be close to the same state as directly after the supernova explosion. In addition, SN 1006 has a low interstellar extinction, which eases the determination of stellar parameters. These serendipitous conditions for the SN 1006 remnant led us to launch a photometric and spectroscopic campaign to search for the donor star. Our photometric observations were taken at Siding Spring Observatory with the 2.3m Telescope imager. The spectroscopic observations were undertaken with the high resolution multi-object spectrograph FLAMES attached to the Very Large Telescope (VLT).

In Section 1.2 we outline the observations as well as data reduction of the photometric and spectroscopic data. Section 1.3 is split into four subsections, namely radial velocity, stellar rotation and stellar parameters. We conclude this chapter in Section 1.4 and discuss the possible implications of our initial find as well as outlining some future work.

1.2. Observations and Data Reduction

1.2.1. Photometric Observations

Charged coupled device (CCD) images of SN 1006 were obtained using the imaging camera at the Nasmyth-B focus of the ANU 2.3 m Telescope at the Siding Spring Observatory, on 11 May 2004. We exposed for 1860 s in U-Band, 1490 s in B-Band, 788 s in V-Band and 1860 s in I-Band. For calibration purposes we took images of the PG1633 and PG1047 standard star regions in the same filters. The seeing ranged between 1''and 2'', and the conditions were photometric. The data were bias corrected and flatfielded (using skyflats) using PyRAF [1].

For our photometric data reduction we fitted an astrometric solution using astrometry from the 2MASS point source catalogue (Skrutskie et al., 2006) to our frames. We used SExtractor (Bertin & Arnouts, 1996) to measure the magnitudes of the objects in the frames and then calibrated our photometry to a standard Bessell Filter system using the Stetson magnitudes [2] of our standard fields PG1633 and PG1047 .

The measured magnitudes were supplemented with near infrared magnitudes from the 2MASS point source catalogue (see Table 2.2 and 2.1). Subsequently we checked the photometric measurements, by plotting the obtained $B - V$ colours against the $V - K$ colours (see Figure 1.1).

We have also computed temperatures from photometric colours by using the polynomials given in Casagrande et al. (2010). In the first instance, we assumed a solar metallicity

[1] PyRAF is a product of the Space Telescope Science Institute, which is operated by AURA for NASA.

[2] This research used the facilities of the Canadian Astronomy Data Centre operated by the National Research Council of Canada with the support of the Canadian Space Agency

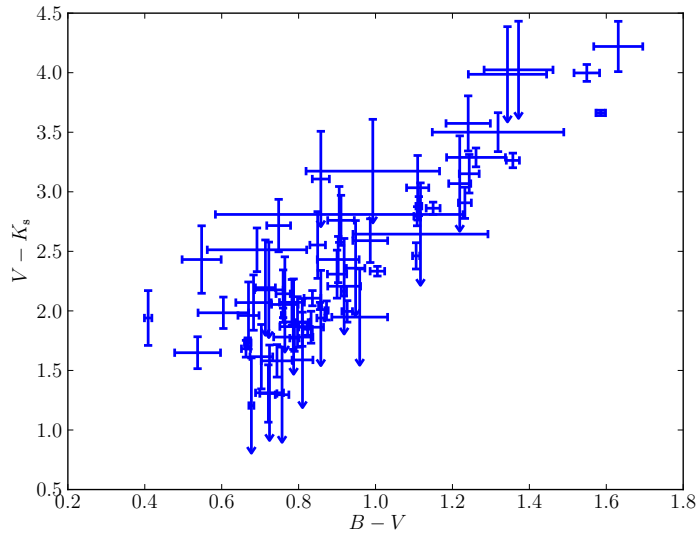

Figure 1.1 Colour-colour plot of all candidates in SN 1006 to check photometry. The correspondence is as expected given the uncertainties in the measurements.

for all stars, but the choice of metallicity only has a minor influence on the temperature calculation (e.g. change of 300K between [Fe/H]=0 and [Fe/H]=-1) for the temperature. In addition, the temperature polynomial coefficients incorporating the metallicity are particularly small for the $V - K$ colour. All temperatures are listed in the optical photometry Table 2.1 and infrared photometry Table 2.2.

1.2.2. Spectroscopic Observations

For the spectroscopy survey we used the VLT instrument FLAMES, which can provide high resolution (R=25,000) optical spectra over a 25′ field of view for up to 130 objects. In this mode, the spectral coverage is limited to 200 Å, and we chose the wavelength region from 5139 Å to 5356 Å which contains the gravity sensitive Mg I b Triplet as well as many iron lines to accurately measure metallicity .For the centre of our spectroscopic survey we chose the mean of the X-ray and radio centre ($\alpha = 15^h02^m22\overset{s}{.}1$ $\delta = -42°05'49''$; Winkler et al., 2003). We chose a search radius of 120′′ - corresponding to the motion of a star travelling 1250 km s^{-1}at 2.2 kpc over 1000 years. This generous choice, which is more than four times our maximum expected escape velocity (see Figure **??** on page ??), was made to accommodate any errors in the choice of the centre. Although the models predict the surviving companion to be several hundred $L_\odot$ (Marietta et al., 2000), we chose a limiting magnitude of $V = 17.5$ (0.5 $L_\odot(V)$ at 2.2 kpc including extinction of E(B-V)=0.1) to accommodate a wide range of potential donor stars. An exposure time of 3.8 hours was chosen to obtain spectra with high enough quality to measure rotation and basic stellar parameters (S/N ratio > 20). For completeness and to not waste fibres we chose additional stars down to a magnitude limit of $V = 19$, which are only used in radial velocity measurements. These constraints yielded 26 stars with $V < 17.5$ and 53 stars in the bin between $17.5 < V < 19$ (for a total of 79 stars) for our survey (see Figure 1.2). With fibre buttons not being able to be placed less than 11′′ apart, we had to split our candidates over

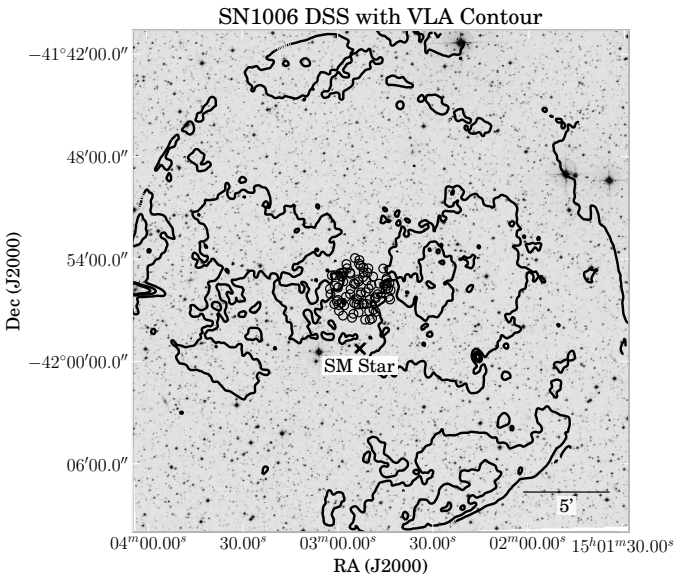

Figure 1.2 Optical DSS image with radio contour overlay (VLA). The black circles in the centre show the 79 program stars. Additionally we have marked the 'spurious' donor the SM-Star.

three different setups. The first two setups were observed five times with 2775 seconds each. We deliberately chose bright stars for the last setup so that it only had to be observed three times with 2775 s each. In addition, we placed spare fibres on three bright stars (R≈ 10; 2MASS J15032744-4204463, 2MASS J15031746-4204165, 2MASS J15033195-4202356) located close to the edge of the 25′ field of view for calibration purposes. Additional spare fibres were placed on sky positions, which were chosen to be far from 2MASS sources and subsequently manually inspected using DSS images to be in star free regions. In addition to our night time calibration, which included simultaneous arc exposures with four fibres for each observation block, we received standard daytime calibrations. In total, 13 observation blocks with an exposure time of 2775 seconds each were obtained. Table 1.1 provides the Observing ID, modified julian date, mean seeing, mean airmass, setup name and heliocentric correction for all observations (all data is available under ESO Program ID: 083.D-0805(A)). Due to broken fibres, not all stars where observed for the expected length of time. Broken fibres caused SN1006-31 not to be observed at all in this project (see Figure 1.3) - although a $V = 17.87$ is not part of our primary sample.

We first applied a cosmic ray removal tool on the raw 2D frames (van Dokkum, 2001). The data was then reduced with the ESO-CPL pipeline (version 5.2.0), using the GIRAFFE instrument recipes (version 2.8.9). The only variation that was made to the default parameters was the usage of the Horne extraction algorithm instead of the "Optimal"-extraction algorithm. This yielded 366 individual spectra of the candidate stars and an additional 39 calibration star spectra.

Table 1.1 Flames Observations of SN1006 program stars

ObsID -	MJD d	FWHM ″	Airmass -	Setup name -	$v_{\rm helio}$ correction km s^{-1}
360737	54965.1	1.2	1.2	SN1006 1	1.5
360739	54965.1	1.2	1.1	SN1006 1	1.5
360740	54965.1	1.0	1.1	SN1006 1	1.4
360741	54985.0	0.7	1.4	SN1006 1	-7.4
360742	54964.2	1.5	1.1	SN1006 1	1.7
360743	54985.0	0.8	1.2	SN1006 2	-7.5
360745	54985.0	0.9	1.1	SN1006 2	-7.6
360746	54985.1	1.0	1.1	SN1006 2	-7.7
360747	54985.1	1.0	1.1	SN1006 2	-7.7
360748	54985.2	0.9	1.1	SN1006 2	-7.8
360749	54963.1	1.2	1.2	SN1006 3	2.4
360751	54963.1	1.1	1.1	SN1006 3	2.3
360752	54963.2	1.1	1.1	SN1006 3	2.3

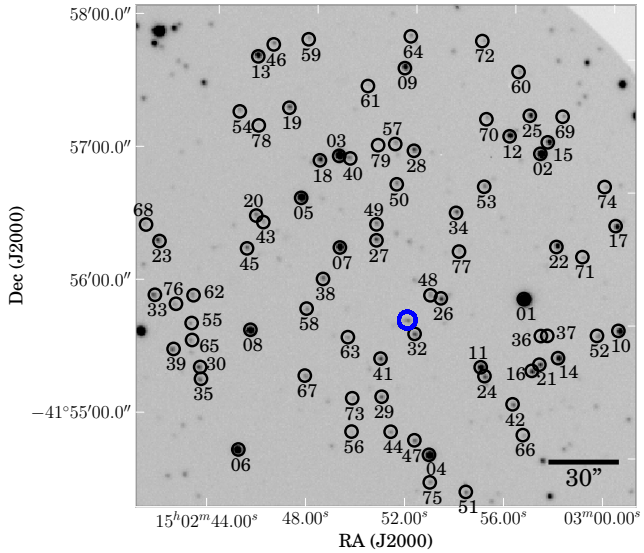

Figure 1.3 V-Band image taken by the 2.3 m Telescope. We have marked SN1006-31, which was not observed due to broken fibres, with a blue circle. With the a brightness of $V = 17.87$ SN1006-31 is fainter than our primary catalog ($V < 17.5$ mag), and is the only star which lacks a spectrum to $V = 19$ in the remnant's centre.

1.3. Analysis

1.3.1. Radial Velocity

To obtain radial velocities we employ a two step process. We used a solar spectrum from Kurucz et al. (1984) with the standard cross-correlation technique described in Tonry

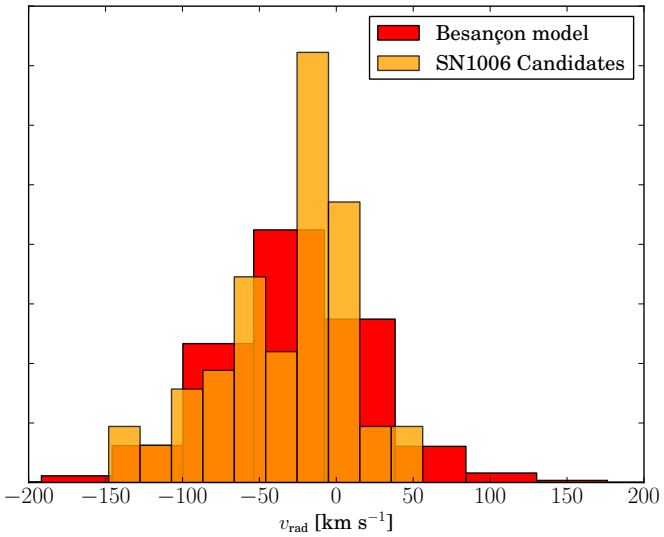

Figure 1.4 Comparison of all candidate stars with the distribution of stars taken from the the Besançon kinematic model. The model input parameters were a search area of 1 square degree around the centre of SN 1006 and a magnitude limit of 10 < V < 17.5

& Davis (1979) and implemented in the PyRAF task FXCOR. The cross-correlation was performed on each individual spectrum. The results were then heliocentrically corrected, and then averaged for each star with a sigma clipping algorithm (see Table 2.3). We note that especially for faint objects we observe a second cross-correlation peak at 0 km s^{-1}and believe that this is reflected sun light from the moon. We believe that this has a negligible effect on our radial velocity measurement. In Figure 1.4 we have compared our radial velocity measurements with the Besançon kinematic model of the Milky way (Robin et al., 2003). Our selection criteria for creating the Besançon kinematic model was all stars within 1 square degree of SN 1006 and a magnitude cut of 10 < V < 17.5. We compared the resulting 10000 stars to our 78 stars in the sample in Figure 1.4.

1.3.2. Rotational Velocity

Due to the direction looked through the Galaxy, there is a large velocity spread in the direction of SN 1006 (see Figure 1.4) making it hard to isolate a donor star based just on kinematic features. A distinguishing feature for a donor star should be rotation (discussed in Chapter **??**), especially if the donor star isn't a giant. The rotational velocities in Chapters **??** & **??** were all measured manually. In these previous measurements we selected weak iron lines and stacked them to obtain a line profile, which was compared to synthetically rotationally broadened lines. This was a feasible way for six spectra, it is however not feasible for more than 200 spectra.

Measuring repetitive structures like line profiles is much more straight forward in Fourier space. The intrinsic spectrum ($f_{\rm spectrum}$) of a star is broadened by a convolution of the intrinsic spectrum with a rotational broadening kernel ($g_{\rm rotation}$). The next broadening is introduced by the instrument (instrumental kernel $h_{\rm instrument}$) before being recorded on the detector. Assuming an unbroadened synthetic spectrum ($f_{\rm synthetic}$), matching the

intrinsic stellar spectrum, we can describe a convolution in Fourier space as,

$$f_{\text{observed}} = f_{\text{spectrum}} \otimes \underbrace{g_{\text{rotation}} \otimes h_{\text{instrument}}}_{f_{\text{profile}}}$$

$$F(f_{\text{spectrum}} \otimes g_{\text{rotation}} \otimes h_{\text{instrument}}) = F(f_{\text{spectrum}}) \times F(g_{\text{rotation}}) \times F(h_{\text{instrument}})$$

$$\Rightarrow \frac{F(f_{\text{observed}})}{F(f_{\text{synthetic}})} \approx F(f_{\text{profile}}),$$

where F denotes the Fourier transform. This yields the line profile which we can separate, knowing the resolution of the instrument, into an instrumental profile and a rotational kernel . This technique has been described by a selection of authors (e.g. Gray, 1977). FXCOR uses this technique to measure radial velocities from shift of the profile peak relative to rest. We have applied this technique successfully to extract the rotation for some of the stars were the quality of the spectra was adequate (see Table 2.3).

1.3.3. Stellar Parameters

We obtained detailed stellar parameters for the donor candidates with $V < 17.5$ by employing a grid based technique (three dimensional grid in T_{eff}, $\log g$ and [Fe/H]). MOOG (Sneden, 1973) was used to synthesise the spectral grid using the model stellar atmospheres by Castelli & Kurucz (2003). Line wings were taken into account up to 8 Å away from line centre, which seemed to be a reasonable compromise between grid creation time and accuracy. For the atomic lines we merged values from the Vienna Atomic Line Database (VALD; Kupka et al., 2000) with adjusted values (to reproduce the Arcturus and the Sun) from Gustafsson et al. (2008). In addition, we used the measured molecular lines described in Kurucz & Bell (1995). The final grid extends from 3500 K to 7500 K in effective temperature with a step size of 250 K, in surface gravity it ranges from 0 to 5 with a stepsize of 0.5 and in [Fe/H] it ranges from -2.5 to 0.5 with a stepsize of 0.5 (with an extra set of points at 0.2).

We used the appropriate sections from the Solar spectrum (Kurucz et al., 1984) and the Arcturus spectrum (Hinkle et al., 2000) to calibrate our spectral grid. We measured stellar parameters by first finding the best fitting grid point and then using the minimizer MINUIT to find a minimum by interpolating between the gridpoints (described in Appendix **??** of this thesis; Barber et al., 1996). For the Sun we obtain stellar parameters of T_{eff}=5825 K, $\log g$=4.4 and [Fe/H]=-0.12 and for Arcturus we obtain stellar parameters of T_{eff}=4336 K, $\log g$=1.9, [Fe/H]=-0.67. We acknowledge the error in measurement, but believe our spectral grid to be accurate enough for distinguishing a potential donor candidate against an unrelated star.

To measure our observed spectra we first fitted the continuum with *Legendre polynomials* with a maximum order of 3 and a sigma clipping algorithm discarding the lines. The order that gave the lowest RMS of the fit was used. We then combined the spectra using the previously measured radial velocity and the computed heliocentric correction. In addition, we broadened the synthetic spectral grid with a rotational kernel for each star where applicable. These spectra were then fitedt using the previously described algorithm, except that we added the $B - V$ photometric temperature as a prior. As the photometric temperature uses the metallicity as an input parameter we recalculated the photometric temperature prior using the metallicity determined by the fit. This procedure was repeated

Table 1.2 SN 1006 candidates ($V < 17.5$) stellar parameters

Name	$T_{\rm eff}$ K	$\log g$ dex	[Fe/H] dex	V mag	$v_{\rm rot}$ km s^{-1}
01	4285	2.0	−1.0	13.50	< 10
02	4001	0.8	−1.4	15.37	< 10
03	5446	4.0	−0.6	15.04	< 10
04	5347	4.0	−0.6	15.47	< 10
05	5191	3.7	−0.6	15.50	< 10
06	5874	4.5	−0.7	15.50	< 10
07	4884	4.2	−0.8	15.90	< 10
08	5954	4.2	−0.5	15.86	< 10
09	4217	3.9	−2.5	16.58	< 10
10	5662	4.3	−0.8	16.30	10
11	5489	4.1	−0.8	16.33	< 10
12	5313	4.4	−0.9	16.39	16
13	5114	4.0	−0.7	16.49	< 10
14	5245	4.3	−0.7	16.56	< 10
15	5503	4.2	−0.7	16.63	< 10
16	4448	4.0	−1.8	17.26	14
17	5515	4.4	−1.2	16.66	< 10
18	5341	4.1	−0.9	16.77	12
19	3846	4.1	−2.4	17.39	17
21	4510	3.1	−1.3	17.36	13
22	6448	4.2	−0.4	16.71	13
23	4429	4.0	−1.8	17.39	14
25	6119	4.9	−0.7	17.03	< 10
26	5619	4.0	−1.1	17.23	< 10
27	5336	4.0	−1.3	17.47	< 10
28	5379	4.3	−1.1	17.43	< 10

until the gravity estimate converged to less than 0.1 dex. We believe our temperatures to be good to a few hundred K, our surface gravities as well as metallicities have a systematic uncertainty of roughly 0.5 dex.

The stellar parameters can be seen in Figure **??** and in tabulated form in Table 1.2. The final set of stellar parameters shows a typical distribution of many dwarfs and a few giants. None of the stars seem to be unusual in any way. In addition both giants, using theoretical absolute magnitudes, have been calculated to be located behind the remnant.

1.4. Conclusions

In this work we have scrutinised all stars to a limit of 0.5 $L_{\odot}(V)$ at the distance of the SN 1006 remnant. None of the stars scrutinised in our sample show features consistent with those expect for donor star models.

Giant star progenitors are ruled out primarily because there is no star luminous enough to be donor star and all giants in our set are located behind the remnant. Marietta et al. (2000) suggests that giant donors have a luminosity of $\approx 1000\,L_\odot$ ($V \approx 9$ at the distance of the remnant) for at least 100,000 years. Furthermore the giant donor would have a very high temperature of more than $10^4\,K$. Some rotation in excess of what has been measured for this sample is expected. None of the giant stars resemble the estimated giant donor post-explosion.

Sub giant donors should also be very luminous (Marietta et al., 2000) with a minimum expected luminosity of $L \approx 500\,L_\odot$ ($V \approx 9.7$ at the distance of the remnant) lasting for 1400–11,000 years. While they might have a radial velocity which could be masked by the large expected dispersion in the direction of SN 1006, the expected $v_{\rm rot} \approx 80\,{\rm km\ s^{-1}}$ (see Figure **??** on page ?? and Figure 1.5), far exceeds any star in our sample.

Finally, main sequence stars, according to Marietta et al. (2000) are expected to have a similar brightness to sub giant stars. Furthermore main sequence donors should have both substantial spatial motion coupled with very high rotation (see Figure **??** on page ?? and Figure 1.5). No star shows any of these features in our sample.

There are however two main caveats. Firstly, rotation can be lost due to expansion (see Section **??**). This, however is apriori unlikely (priv. comm. Chris Tout). Secondly, measurements by Winkler et al. (2005, see Figure 1.6)cast doubt on a precise determination of the centre. Their research suggests that the centre of the iron core is offset from the geometric centre determined by the shocked interstellar medium (ISM). However, we argue that this does not mean that the centre of mass (where a donor star would reside) is necessarily off centre. In fact, Maeda et al. (2010) suggest that the iron ejecta is offset from the centre of mass, which suggests that the centre of the iron core will be different than the centre of mass. This caveat is probably not easily resolved and we will have to hope that our generous choice in radius around the geometric centre incorporates any such errors. In addition, other groups are also currently surveying SN 1006 with a spatially larger but photometrically shallower field (priv. comm. Pilar Ruiz-Lapuente) and have not yet found a viable companion. In summary our research shows a consistent result to SN 1572 - no identifiable donor star.

The observations presented here for SN 1006 are in conflict with the standard SN Ia donor star scenarios, which include accretion onto a white dwarf from a main sequence, sub giant, or giant companion. A few non-standard scenarios survive our observational tests. These include a helium white dwarf as a donor star (see Section **??**), which would not be detectable with our observations, although it is unlikely that a helium white dwarf would survive the explosion (priv. comm. Rüdiger Pakmor). The other possibility is that SNe Ia (or at least SN 1006 and SN 1572) do not have donor stars, consistent with a double degenerate scenario (DD-scenario).

Another remnant that can be subjected to such an intensive search is Kepler (SN 1604). Kepler seems to be different from either SN 1572 and SN 1006 due to detection of interaction with the circumstellar medium (CSM). Observational facts of the Kepler remnant as well as the description of the donor star search will be discussed in the conclusion of this thesis (Chapter **??**).

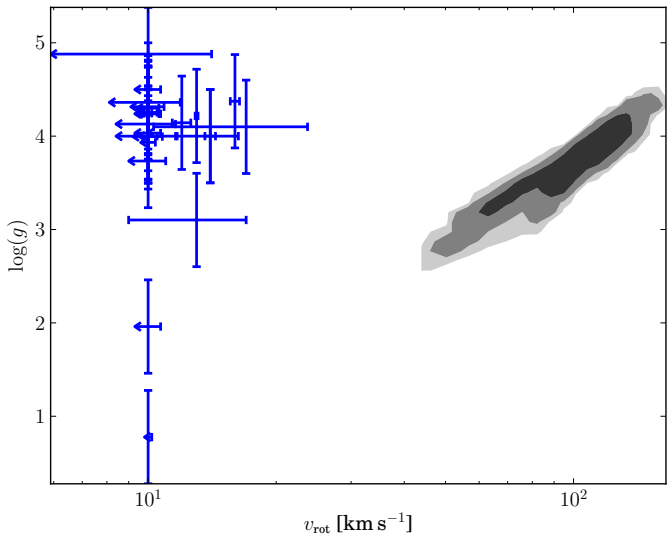

Figure 1.5 Comparison of the evolutionary state and rotational velocity of 55000 binary synthesis SD-Scenario progenitors (gray shades;data from Han, 2008) with the measured rotation from this work. Due to the resolution of the spectrograph most of these stars only have an upper limit of the rotation speed of $v_{\rm rot}$ = 10 km s^{-1}

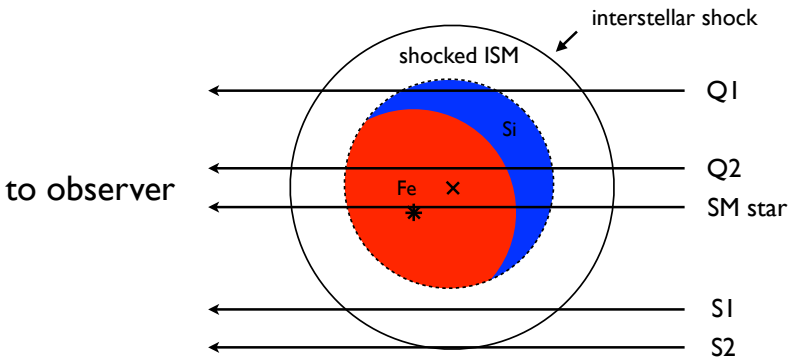

Figure 1.6 Background UV sources probing the remnant. Figure adapted from Winkler et al. (2005)

CHAPTER 2

SN 1006 Data

Table 2.1 SN 1006 optical photometry (Candidates with $V < 17.5$ marked with gray)

Star	RA	Dec	U	σ_U	B	σ_B	V	σ_V	I	σ_I
	hh:mm:ss.ss	dd:mm:ss.ss	mag	mag	mag	mag	mag	mag	mag	mag
01	15:02:58.27	-41:55:20.9	16.03	0.02	14.76	0.00	13.50	0.08	12.30	0.18
02	15:02:59.95	-41:56:25.2	18.84	0.08	16.96	0.01	15.37	0.01	13.95	0.05
03	15:02:51.80	-41:56:39.9	16.16	0.02	15.86	0.01	15.04	0.01	14.23	0.09
04	15:02:53.35	-41:54:18.0	16.67	0.02	16.33	0.00	15.47	0.00	14.62	0.00
05	15:02:49.97	-41:56:23.9	16.90	0.03	16.41	0.00	15.50	0.01	14.65	0.00
06	15:02:45.68	-41:54:35.2	16.21	0.01	16.17	0.01	15.50	0.00	14.78	0.01
07	15:02:51.19	-41:55:58.5	17.62	0.05	16.91	0.02	15.90	0.01	14.92	0.02
08	15:02:47.00	-41:55:28.3	16.57	0.03	16.53	0.01	15.86	0.01	15.16	0.00
09	15:02:55.07	-41:57:14.4	18.46	0.20	17.73	0.01	16.58	0.01	15.53	0.02
10	15:03:01.87	-41:54:59.2	17.18	0.04	17.06	0.00	16.30	0.00	15.51	0.00
11	15:02:56.05	-41:54:53.5	17.02	0.03	17.12	0.00	16.33	0.05	15.61	0.01
12	15:02:58.83	-41:56:35.5	17.60	0.03	17.22	0.00	16.39	0.02	15.50	0.02
13	15:02:49.22	-41:57:31.1	17.93	0.09	17.41	0.01	16.49	0.00	15.74	0.06
14	15:02:59.24	-41:54:51.6	17.93	0.04	17.44	0.00	16.56	0.00	15.75	0.01
15	15:03:00.33	-41:56:29.8	17.81	0.01	17.42	0.01	16.63	0.01	15.87	0.04
16	15:02:58.09	-41:54:47.9	19.60	0.47	18.37	0.01	17.26	0.00	16.11	0.03
17	15:03:02.49	-41:55:46.7	17.45	0.02	17.40	0.00	16.66	0.04	16.02	0.13
18	15:02:50.99	-41:56:39.4	18.00	0.03	17.61	0.00	16.77	0.03	15.87	0.04
19	15:02:50.12	-41:57:05.5	20.28	0.00	18.75	0.01	17.39	0.01	16.01	0.00
20	15:02:48.03	-41:56:19.4	-	-	19.59	0.03	18.04	0.01	15.97	0.17
21	15:02:58.44	-41:54:50.1	20.60	0.00	18.47	0.01	17.36	0.01	16.30	0.03
22	15:02:59.95	-41:55:41.9	17.26	0.04	17.25	0.00	16.71	0.06	16.18	0.04
23	15:02:43.94	-41:56:15.4	19.62	0.32	18.50	0.01	17.39	0.00	16.24	0.01
24	15:02:56.14	-41:54:49.2	-	-	18.28	0.00	17.59	0.13	16.49	0.11
25	15:02:59.79	-41:56:43.2	17.75	0.01	17.64	0.06	17.03	0.02	16.35	0.03
26	15:02:54.92	-41:55:27.7	18.10	0.10	17.95	0.01	17.23	0.02	16.43	0.00
27	15:02:52.72	-41:55:58.9	18.61	0.08	18.26	0.02	17.47	0.03	16.64	0.05
28	15:02:54.86	-41:56:36.4	18.52	0.13	18.24	0.00	17.43	0.02	16.70	0.02

Table 2.1 – continued from previous page

Star	RA	Dec	U	σ_U	B	σ_B	V	σ_V	I	σ_I
	hh:mm:ss.ss	dd:mm:ss.ss	mag	mag	mag	mag	mag	mag	mag	mag
29	15:02:51.84	-41:54:47.9	-	-	19.23	0.00	18.00	0.02	16.72	0.04
30	15:02:44.71	-41:55:15.4	18.05	0.03	18.24	0.03	17.54	0.02	16.75	0.01
32	15:02:53.61	-41:55:13.7	18.72	0.18	18.42	0.02	17.64	0.03	16.78	0.03
33	15:02:43.38	-41:55:51.5	19.07	0.23	18.56	0.04	17.66	0.04	16.69	0.05
34	15:02:56.13	-41:56:05.1	18.64	0.11	18.52	0.02	17.76	0.01	16.94	0.01
35	15:02:44.66	-41:55:10.0	19.06	0.17	18.74	0.00	17.84	0.02	16.88	0.05
36	15:02:58.70	-41:55:02.9	19.46	0.40	18.65	0.01	17.79	0.01	16.86	0.02
38	15:02:50.29	-41:55:45.6	18.58	0.08	18.48	0.03	17.80	0.03	17.00	0.01
39	15:02:43.76	-41:55:25.6	18.86	0.06	18.44	0.02	17.69	0.01	16.97	0.01
40	15:02:52.23	-41:56:37.9	-	-	-	-	-	-	16.28	0.06
41	15:02:52.06	-41:55:05.2	17.97	0.01	18.02	0.00	17.61	0.01	17.11	0.02
42	15:02:57.08	-41:54:34.3	19.22	0.27	18.78	0.03	17.99	0.01	17.16	0.03
43	15:02:48.27	-41:56:15.9	-	-	20.14	0.04	18.76	0.08	17.25	0.06
44	15:02:51.96	-41:54:31.4	-	-	19.79	0.01	18.54	0.02	17.06	0.01
45	15:02:47.43	-41:56:05.3	18.45	0.11	18.43	0.02	17.71	0.03	17.00	0.05
46	15:02:49.93	-41:57:35.3	20.09	0.17	19.04	0.03	18.05	0.04	17.19	0.20
47	15:02:52.86	-41:54:25.7	18.89	0.24	18.63	0.01	17.96	0.03	17.14	0.03
48	15:02:54.52	-41:55:29.9	-	-	19.29	0.03	18.38	0.01	17.38	0.06
49	15:02:52.83	-41:56:06.1	18.90	0.33	18.84	0.00	18.17	0.01	17.37	0.05
50	15:02:53.93	-41:56:22.6	19.68	0.11	18.99	0.03	18.07	0.03	17.19	0.02
51	15:02:54.58	-41:53:58.4	19.47	0.00	18.90	0.26	17.99	0.19	16.93	0.17
52	15:03:00.97	-41:54:58.6	19.41	0.17	18.89	0.00	18.08	0.03	17.24	0.02
53	15:02:57.45	-41:56:14.7	19.32	0.43	18.90	0.03	18.13	0.01	17.24	0.05
54	15:02:48.09	-41:57:07.7	20.33	0.58	19.40	0.02	18.45	0.01	17.48	0.03
55	15:02:44.67	-41:55:35.9	-	-	19.90	0.01	18.68	0.03	17.36	0.04
56	15:02:50.38	-41:54:34.5	-	-	20.15	0.16	18.83	0.06	17.46	0.08
57	15:02:54.15	-41:56:40.9	19.59	0.57	18.91	0.02	18.26	0.04	17.63	0.07
58	15:02:49.42	-41:55:33.5	18.90	0.09	18.92	0.02	18.21	0.02	17.41	0.02
59	15:02:51.38	-41:57:34.9	19.59	0.37	19.21	0.01	18.54	0.02	17.78	0.02
60	15:02:59.64	-41:57:03.8	20.05	0.18	19.22	0.01	18.48	0.13	18.62	0.43
61	15:02:53.45	-41:57:09.2	-	-	20.49	0.05	19.24	0.02	17.82	0.07
62	15:02:44.94	-41:55:48.3	-	-	19.38	0.02	18.53	0.01	17.54	0.01
63	15:02:50.89	-41:55:17.4	20.19	0.15	19.41	0.00	18.55	0.02	17.62	0.05
64	15:02:55.53	-41:57:28.3	19.45	0.28	18.87	0.02	18.51	0.03	17.87	0.08
65	15:02:44.57	-41:55:28.2	18.79	0.04	18.93	0.03	18.38	0.04	17.63	0.05
66	15:02:57.28	-41:54:19.6	-	-	20.02	0.03	19.09	0.02	18.00	0.03
67	15:02:48.88	-41:55:03.4	19.69	0.38	19.11	0.03	18.37	0.01	17.57	0.01
68	15:02:43.51	-41:56:23.9	20.65	0.00	19.60	0.04	18.75	0.04	17.94	0.01
69	15:03:01.11	-41:56:40.2	20.07	0.00	19.59	0.03	18.59	0.17	17.91	0.09
70	15:02:58.01	-41:56:45.0	20.38	0.57	19.49	0.01	18.73	0.03	18.00	0.06
71	15:03:00.93	-41:55:35.3	-	-	19.95	0.02	18.84	0.02	17.92	0.25
72	15:02:58.39	-41:57:20.6	19.34	0.00	19.90	0.11	18.85	0.11	18.01	0.14
73	15:02:50.64	-41:54:49.5	-	-	20.00	0.04	19.04	0.06	17.92	0.12

Table 2.1 – continued from previous page

Star	RA	Dec	U	σ_U	B	σ_B	V	σ_V	I	σ_I
	hh:mm:ss.ss	dd:mm:ss.ss	mag	mag	mag	mag	mag	mag	mag	mag
74	15:03:02.32	-41:56:05.2	-	-	19.88	0.08	18.76	0.16	18.21	0.02
75	15:02:53.19	-41:54:05.5	19.23	0.11	19.07	0.03	18.34	0.03	17.50	0.03
76	15:02:44.17	-41:55:45.8	19.56	0.09	19.40	0.02	18.70	0.03	17.91	0.08
77	15:02:55.98	-41:55:47.4	19.58	0.20	19.22	0.02	18.56	0.05	17.69	0.02
78	15:02:48.76	-41:56:59.9	-	-	20.87	0.10	19.53	0.01	18.06	0.05
79	15:02:53.45	-41:56:41.7	-	-	21.53	0.06	19.90	0.02	18.04	0.05

Table 2.2 SN 1006 infrared photometry (Candidates with $V < 17.5$ marked in gray)

Star	J	σ_J	H	σ_H	K	σ_K	QFlag	T_{eff}(B-V)	T_{eff}(V-K)
	mag	mag	mag	mag	mag	mag		K	K
01	11.05	0.02	10.32	0.02	10.21	0.02	AAA	4531	4376
02	12.67	0.03	11.87	0.03	11.71	0.02	AAA	3990	4150
03	13.63	0.04	13.26	0.04	13.19	0.05	AAA	5559	5780
04	13.92	0.03	13.56	0.03	13.43	0.03	AAA	5467	5518
05	13.93	0.02	13.50	0.03	13.33	0.04	AAA	5299	5367
06	14.15	0.02	13.82	0.03	13.77	0.04	AAA	6051	5947
07	14.11	0.03	13.68	0.03	13.57	0.04	AAA	5080	5178
08	14.51	0.03	14.32	0.04	14.18	0.07	AAA	6067	6026
09	14.45	0.03	13.85	0.04	13.72	0.05	AAA	4754	4687
10	14.79	0.03	14.37	0.03	14.34	0.06	AAA	5751	5619
11	14.93	0.05	14.69	0.07	14.55	0.09	AAA	5669	5876
12	14.81	0.04	14.39	0.05	14.28	0.06	AAA	5523	5437
13	14.86	0.04	14.52	0.05	14.49	0.09	AAA	5277	5576
14	15.01	0.04	14.67	0.04	14.56	0.08	AAA	5420	5566
15	15.23	0.04	14.96	0.06	14.86	0.11	AAA	5660	5890
16	15.17	0.07	14.63	0.07	14.47	0.08	AAA	4843	4742
17	15.48	0.06	15.06	0.07	15.08	0.13	AAB	5800	-
18	15.37	0.06	14.99	0.06	14.91	0.13	AAB	5533	-
19	15.00	0.04	14.34	0.05	14.13	0.06	AAA	4356	4393
20	14.92	0.04	14.29	0.05	14.04	0.07	AAA	4044	3978
21	15.41	0.05	14.96	0.06	14.90	0.11	AAB	4849	-
22	15.70	0.07	15.43	0.08	15.06	0.12	AAB	6537	-
23	15.35	0.05	14.76	0.05	14.51	0.08	AAA	4833	4673
24	15.90	0.08	15.22	0.09	15.08	0.13	AAB	5969	-
25	15.56	0.05	15.27	0.06	15.05	0.13	AAB	6278	-
26	16.05	0.09	15.66	0.13	15.92	0.24	ABD	5872	-
27	16.08	0.08	15.59	0.11	15.56	0.21	ABC	5636	-
28	16.08	0.08	15.38	0.09	15.53	0.20	AAC	5600	-
29	15.75	0.06	15.18	0.08	15.09	0.13	AAB	4587	-
30	15.98	0.09	15.72	0.11	15.92	0.27	AAD	5932	-
32	16.17	0.11	15.69	0.12	15.57	0.19	ABC	5680	-
33	16.00	0.08	15.41	0.09	15.23	0.19	AAC	5338	-
34	16.25	0.09	15.54	0.10	15.62	0.20	AAC	5750	-
35	16.08	0.12	15.72	0.12	15.53	0.20	BBC	5346	-
36	16.56	0.13	16.60	0.24	15.85	-	BDU	5461	-
37	-	-	-	-	-	-	-	-	-
38	16.24	0.08	16.03	0.13	15.73	0.23	ABD	5999	-
39	16.28	0.12	16.16	0.15	16.39	-	BCU	5759	-
40	14.96	0.04	14.28	0.04	14.06	0.05	AAA	-	-
41	16.43	0.11	16.02	0.14	15.67	0.23	ABD	7102	-
42	16.30	0.08	15.98	0.14	16.12	-	ABU	5667	-
43	16.39	0.12	15.49	0.08	14.74	-	BAU	4330	-

Table 2.2 – continued from previous page

Star	J	σ_J	H	σ_H	K	σ_K	QFlag	T_{eff}(B-V)	T_{eff}(V-K)
	mag	mag	mag	mag	mag	mag		K	K
44	16.19	0.09	15.39	0.09	15.39	0.16	AAC	4565	-
45	16.59	0.13	15.92	0.12	15.53	-	BBU	5868	-
46	16.52	0.12	15.76	0.12	15.46	0.18	BBC	5125	-
47	16.43	0.11	16.08	0.14	16.00	0.28	ABD	6044	-
48	16.76	0.13	16.04	0.15	15.62	0.21	BBC	5319	-
49	16.72	0.13	16.37	0.18	16.96	-	BCU	6019	-
50	16.59	0.12	15.89	0.14	15.86	-	BBU	5297	-
51	16.72	0.13	16.08	0.15	15.18	0.14	BBB	5331	-
52	16.66	0.12	16.15	0.17	16.49	-	BCU	5598	-
53	16.69	0.13	16.15	0.17	16.08	-	BCU	5736	-
54	16.64	0.13	16.02	-	16.09	-	BUU	5220	-
55	16.50	0.15	15.99	0.14	15.61	-	BBU	4613	-
56	16.54	0.13	15.72	0.13	15.33	0.15	BBC	4425	-
57	-	-	-	-	-	-	-	6120	-
58	16.82	0.15	16.78	0.28	16.01	-	BDU	5897	-
59	-	-	-	-	-	-	-	6017	-
60	-	-	-	-	-	-	-	5816	-
61	16.50	0.12	15.93	0.13	15.67	0.23	BBD	4570	-
62	17.15	0.23	16.10	0.14	15.98	0.28	DBD	5485	-
63	16.95	0.17	16.15	0.15	15.44	-	CCU	5461	-
64	-	-	-	-	-	-	-	7316	-
65	17.20	0.20	16.51	0.22	15.95	0.28	CDD	6495	-
66	-	-	-	-	-	-	-	5274	-
67	16.91	0.18	16.53	0.21	15.65	0.22	CDD	5786	-
68	-	-	-	-	-	-	-	5495	-
69	16.94	0.14	17.68	-	15.42	-	CUU	5109	-
70	-	-	-	-	-	-	-	5774	-
71	16.71	0.14	16.42	0.21	15.81	0.27	CCD	4840	-
72	-	-	-	-	-	-	-	4974	-
73	16.85	0.16	16.11	0.16	17.09	-	CCU	5193	-
74	17.17	0.23	16.00	0.15	16.12	-	DBU	4824	-
75	16.84	0.14	16.73	-	17.03	-	BUU	5862	-
76	-	-	-	-	-	-	-	5947	-
77	-	-	-	-	-	-	-	6074	-
78	17.02	0.19	16.11	0.17	15.54	-	CCU	4381	-
79	16.68	0.13	15.87	0.13	15.68	0.21	BBC	3924	-

Table 2.3 SN 1006 candidate kinematics with statistical errors and number of measurements (candidates with $V < 17.5$ marked in gray)

Name	v_{rad} km s^{-1}	σ_{rad} km s^{-1}	N_{rad}	v_{rot} km s^{-1}	σ_{rot} km s^{-1}	N_{rot}
01	-109.1	0.0	5	< 10	0.7	5
02	56.2	0.4	3	< 10	0.2	3
03	5.9	1.0	3	< 10	0.0	3
04	-14.3	0.0	5	< 10	0.7	5
05	-1.1	0.0	5	< 10	1.0	5
06	-103.9	0.2	5	< 10	0.7	5
07	-76.3	2.1	5	10	0.2	5
08	-0.6	0.2	5	< 10	0.6	5
09	-47.0	0.8	5	< 10	0.4	5
10	-20.2	0.5	5	< 10	0.9	5
11	-5.9	0.3	5	< 10	1.6	5
12	-59.8	0.4	5	16	0.4	5
13	12.3	0.1	5	< 10	1.6	5
14	-17.0	0.4	5	< 10	0.6	5
15	-72.0	0.2	5	< 10	0.7	5
16	9.4	0.1	5	14	2.3	5
17	-102.1	0.3	5	< 10	1.9	5
18	11.6	0.7	5	12	0.6	5
19	-47.8	0.3	5	17	6.7	4
20	-22.4	0.5	4	-	0.0	2
21	-18.5	0.0	5	13	4.0	4
22	-22.9	0.7	2	13	0.1	2
23	-63.3	1.3	5	14	0.4	4
24	-67.2	0.8	5	10	-	1
25	40.7	0.3	5	< 10	4.1	5
26	-7.0	0.1	5	< 10	0.8	5
27	-52.0	2.1	5	< 10	0.5	5
28	-43.5	0.3	3	< 10	0.5	3
29	-13.3	0.2	4	14	2.3	5
30	-28.2	1.3	3	< 10	0.5	3
32	-104.0	0.3	5	11	3.2	3
33	-120.9	0.2	5	< 10	1.3	4
34	-47.1	0.5	5	< 10	3.0	4
35	-24.6	1.5	5	12	0.9	4
36	-96.7	1.2	3	< 10	-	1
37	-22.7	16.1	4	-	-	-
38	-12.4	2.2	5	< 10	0.8	5
39	22.4	1.3	3	< 10	0.8	2
40	-13.8	8.6	4	-	-	-
41	-4.4	4.3	5	16	1.2	4
42	-64.9	0.3	5	< 10	0.5	3
43	-7.6	1.7	5	-	-	-

Table 2.3 – continued from previous page

Name	v_{rad} km s^{-1}	σ_{rad} km s^{-1}	N_{rad}	v_{rot} km s^{-1}	σ_{rot} km s^{-1}	N_{rot}
44	-28.2	0.2	4	-	-	-
45	-135.4	0.3	5	< 10	3.9	4
46	-13.0	0.3	5	11	0.6	2
47	-0.3	0.1	5	< 10	2.7	4
48	3.6	0.6	3	11	1.9	3
49	-90.4	64.7	3	< 10	1.0	3
50	-82.7	1.5	5	< 10	1.0	5
51	-59.8	0.5	5	14	1.2	2
52	-8.8	1.1	4	-	-	-
53	-63.2	1.3	5	< 10	-	1
54	-51.8	0.0	5	10	1.4	2
55	-24.7	1.5	5	-	-	-
56	-0.0	1.9	4	-	-	-
57	-40.7	2.0	4	-	-	-
58	2.0	0.2	5	< 10	1.5	4
59	-17.5	0.4	5	< 10	-	1
60	-73.0	2.2	3	< 10	-	1
61	-34.6	24.7	5	-	0.0	5
62	21.2	1.1	3	12	-	1
63	-45.8	42.1	5	14	2.4	2
64	-24.1	0.4	2	< 10	-	1
65	38.3	55.3	3	< 10	-	-
66	-15.4	13.7	2	-	-	-
67	-146.2	1.1	4	< 10	-	1
68	-71.3	0.5	5	10	-	1
69	-47.6	0.4	5	12	0.1	2
70	-23.9	1.0	5	19	1.8	5
71	0.7	0.1	5	14	2.0	5
72	-4.5	5.9	2	-	-	-
73	-8.0	1.0	4	< 10	2.0	2
74	-27.2	23.0	5	-	-	-
75	-147.9	0.4	5	< 10	0.5	3
76	23.3	24.1	5	-	-	-
77	-3.3	3.8	4	-	-	-
78	-7.5	0.3	5	-	-	-
79	-0.6	4.5	4	-	-	-

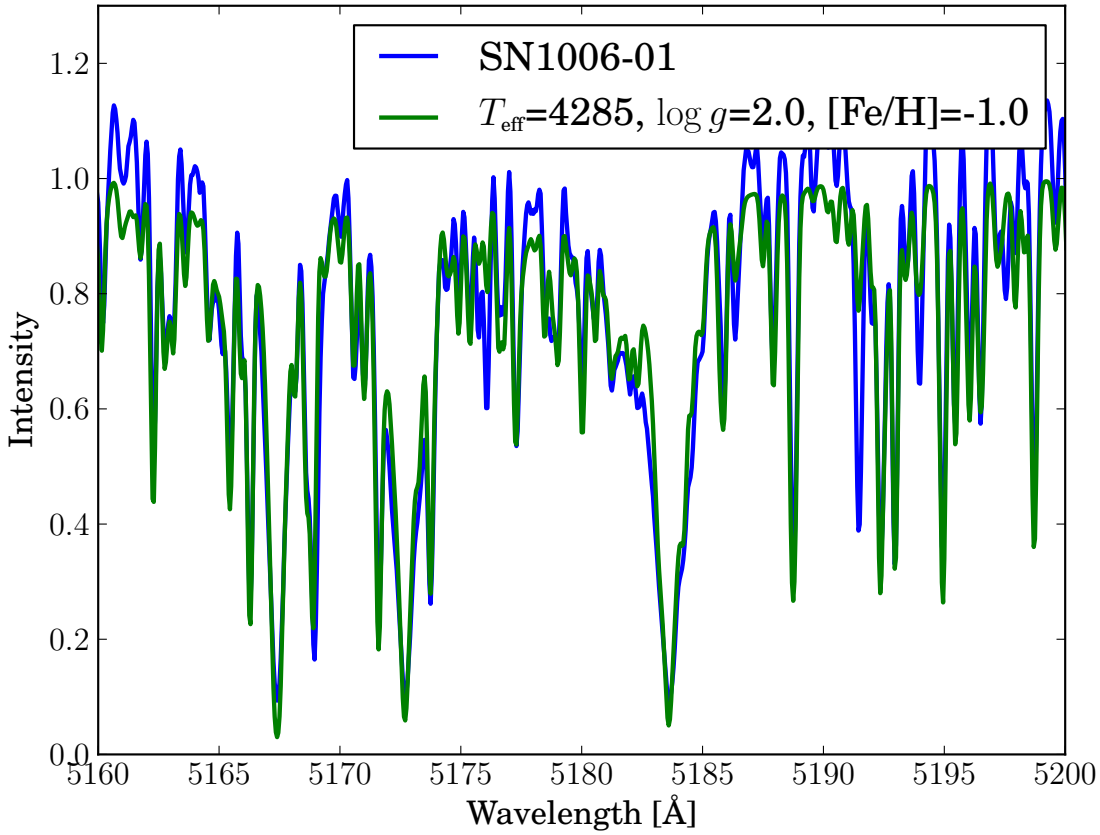

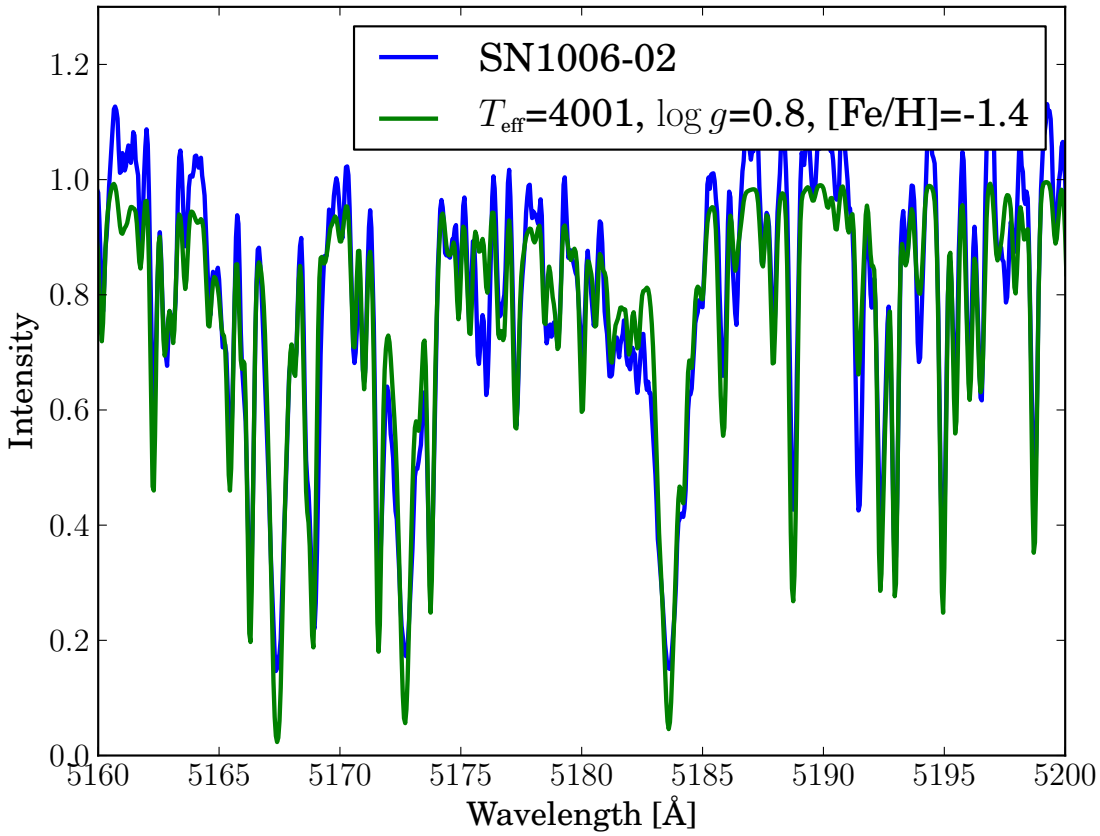

Figure 2.1 Fit of SN 1006 candidate spectra

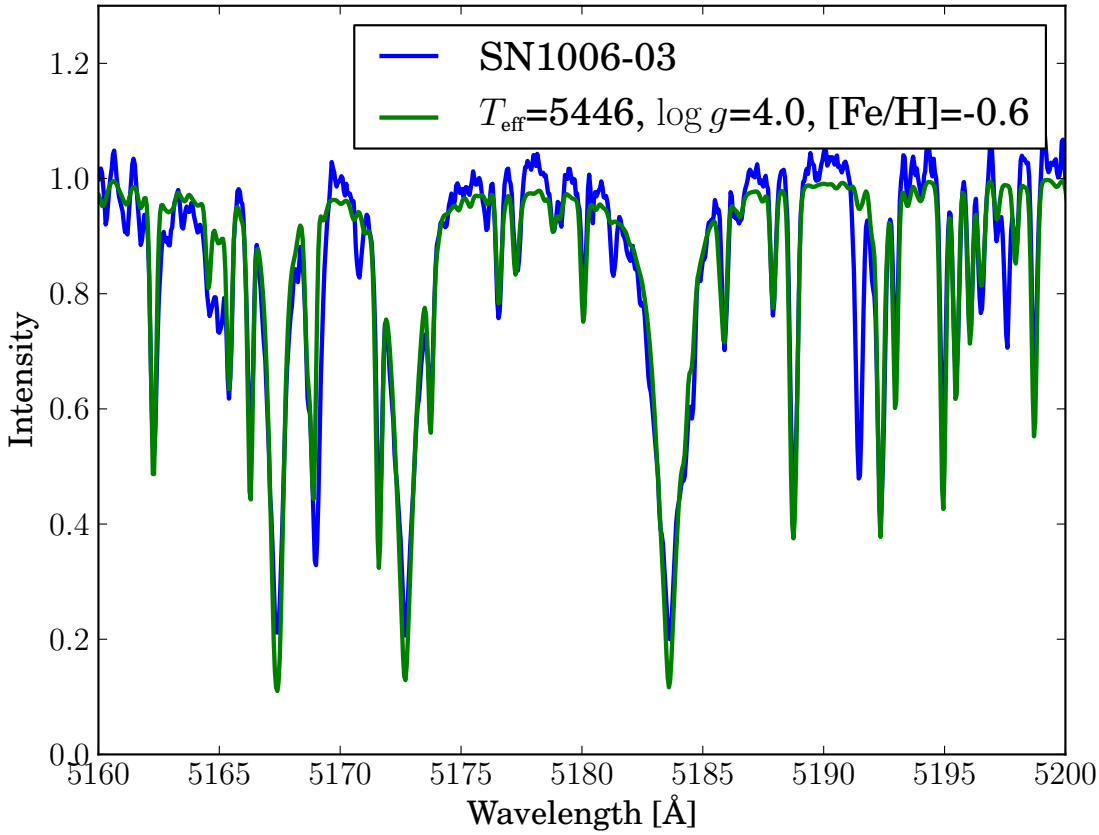

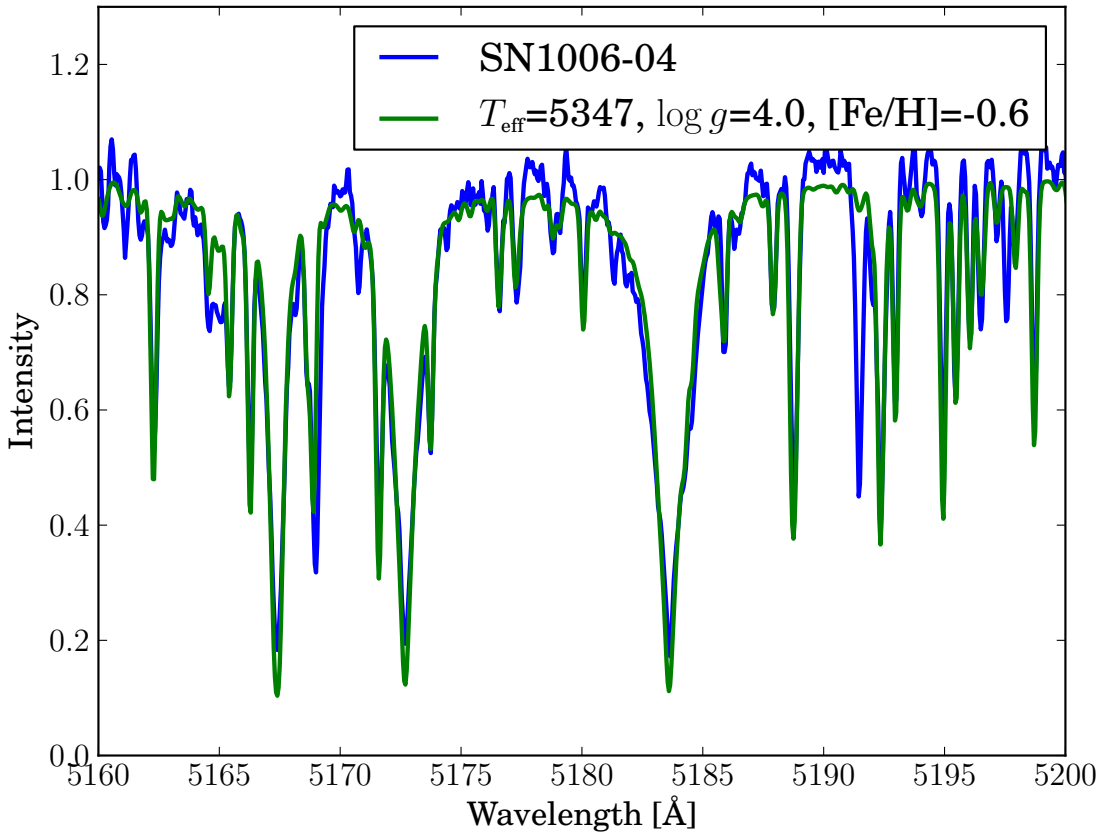

Figure 2.1 Fit of SN 1006 candidate spectra

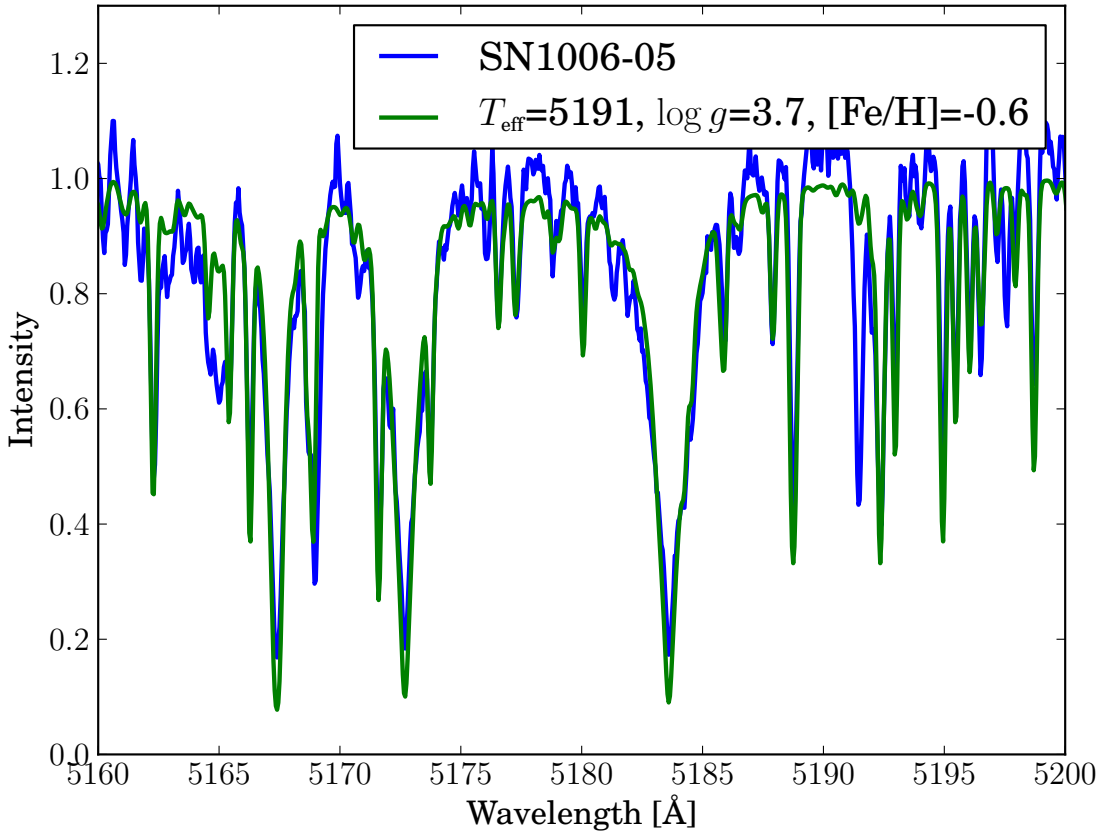

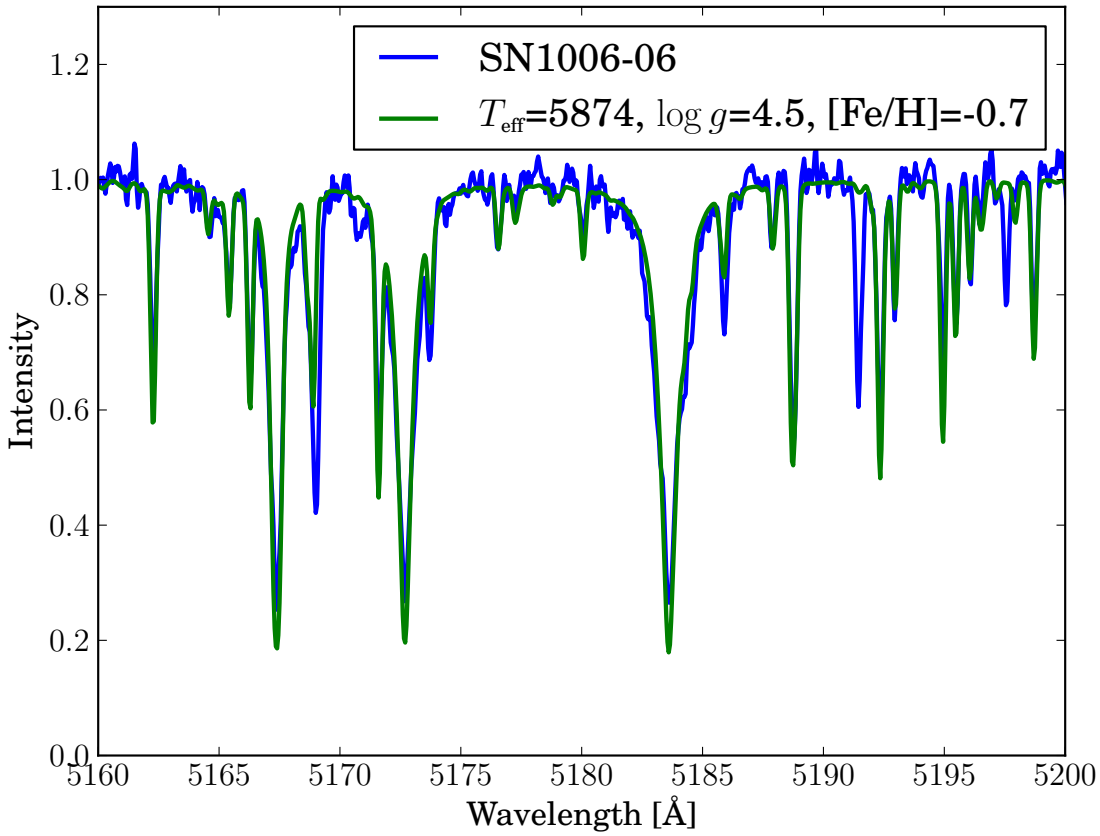

Figure 2.1 Fit of SN 1006 candidate spectra

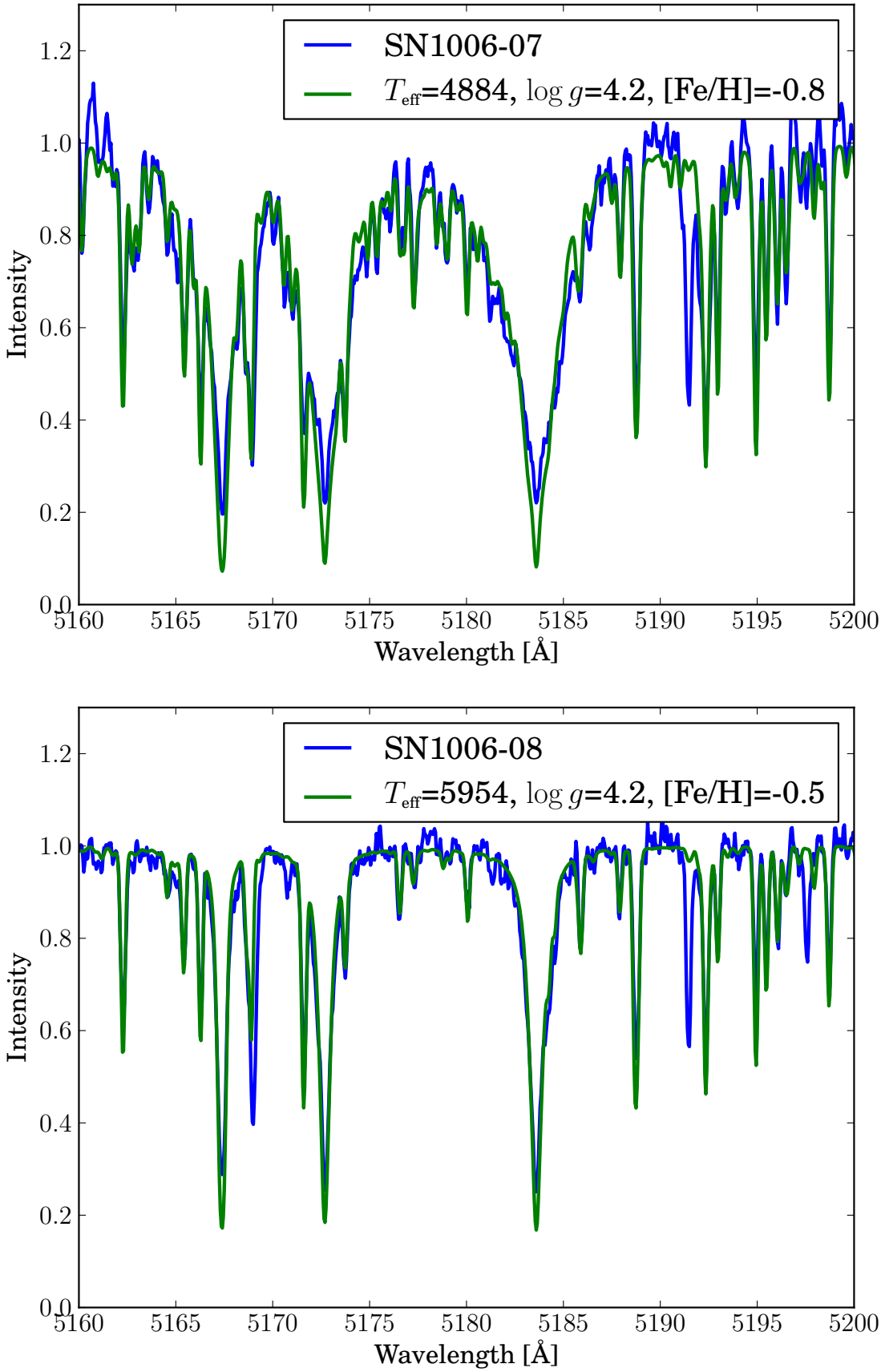

Figure 2.1 Fit of SN 1006 candidate spectra

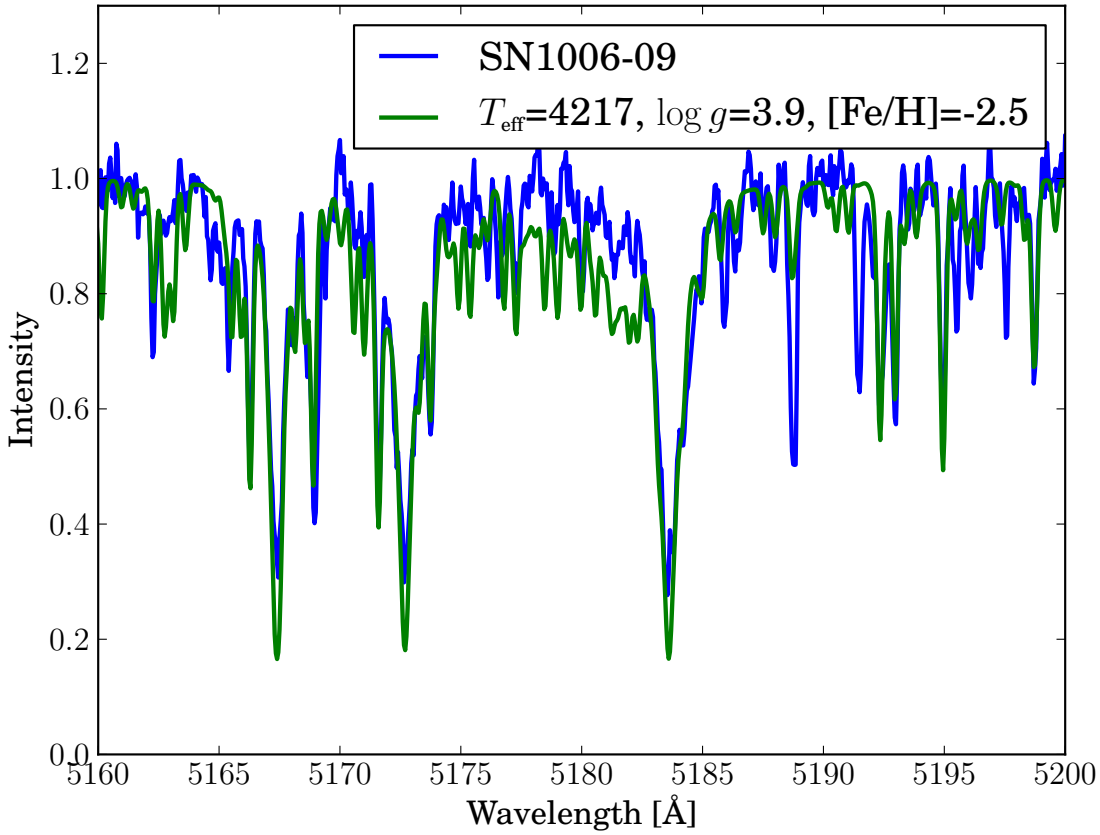

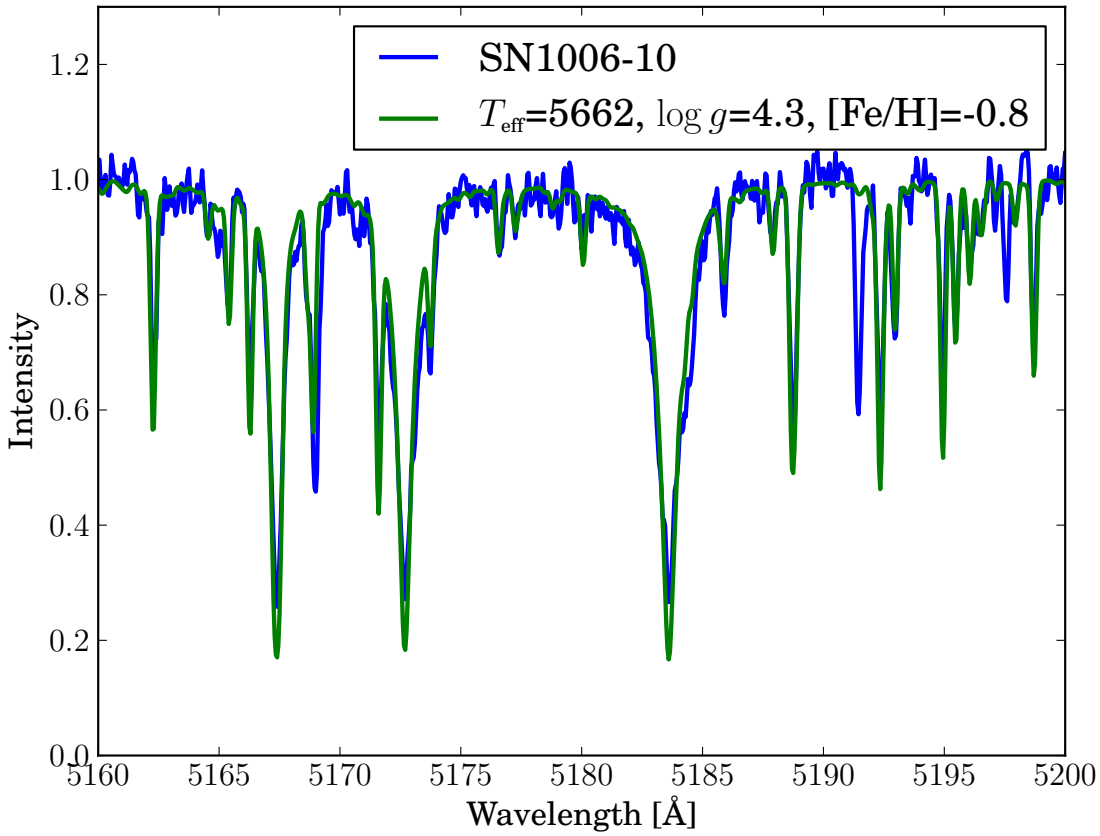

Figure 2.1 Fit of SN 1006 candidate spectra

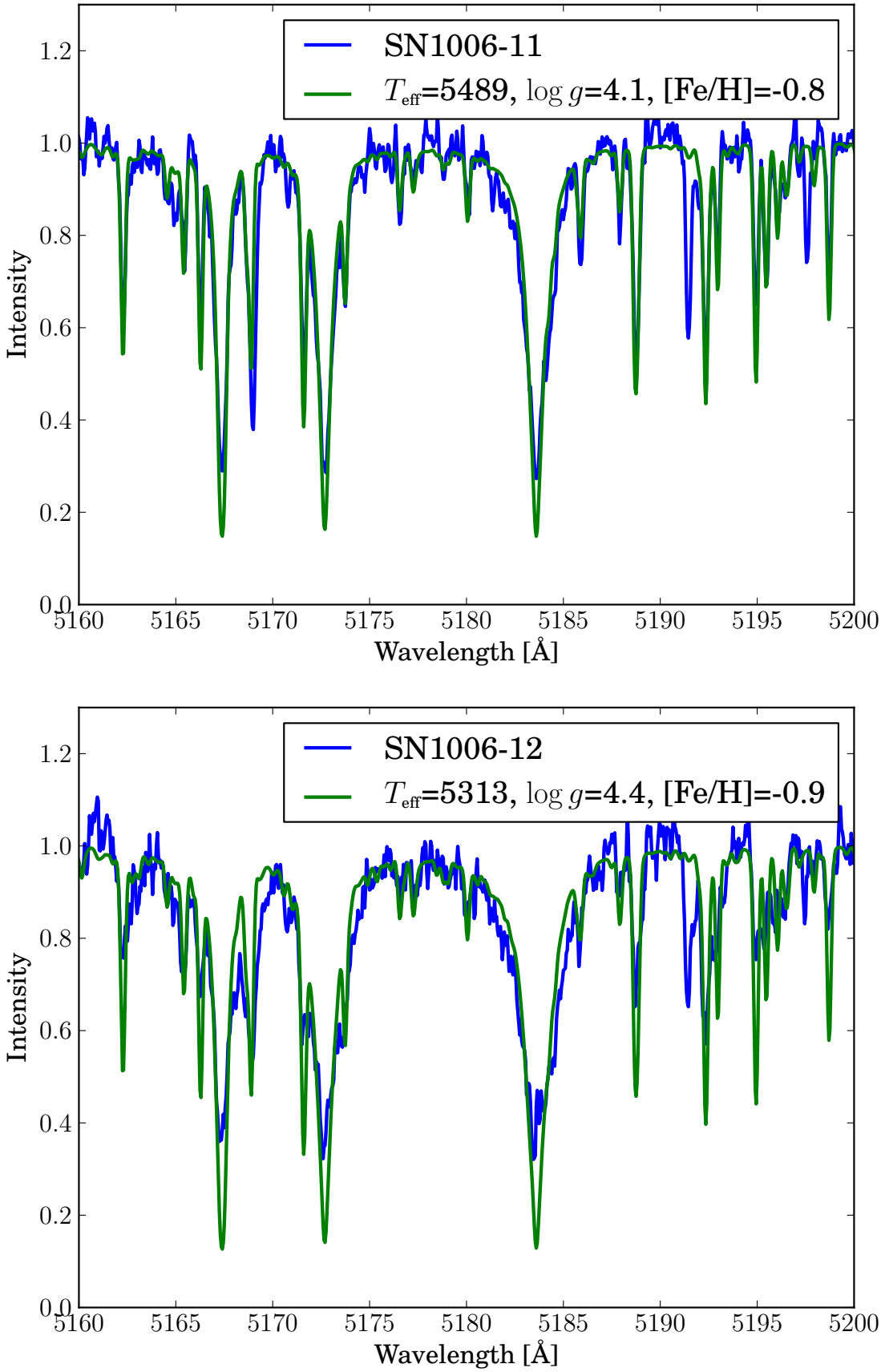

Figure 2.1 Fit of SN 1006 candidate spectra

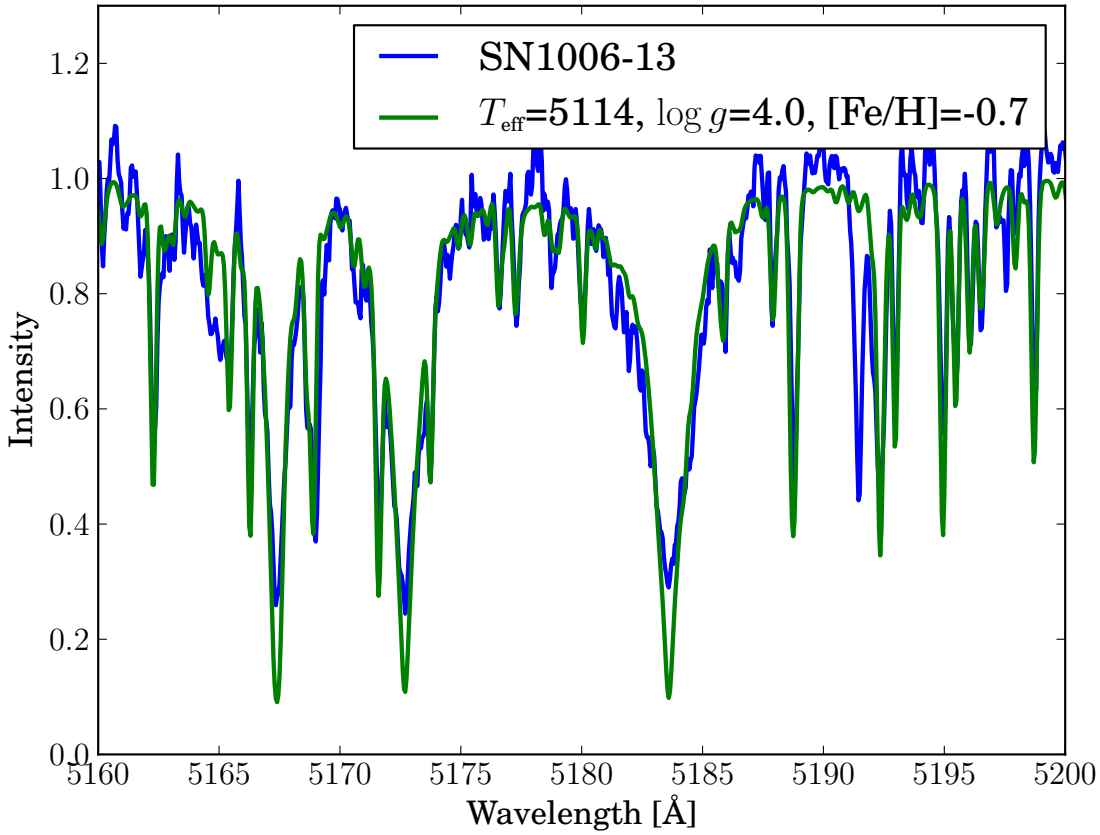

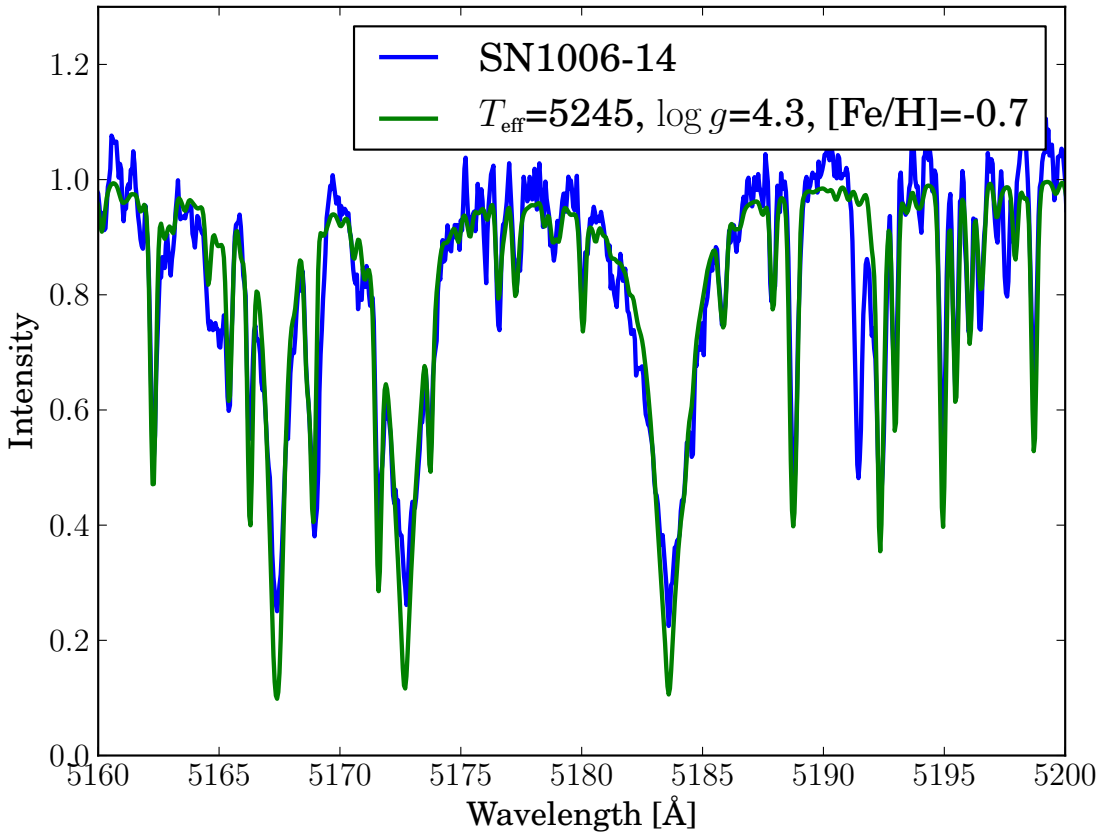

Figure 2.1 Fit of SN 1006 candidate spectra

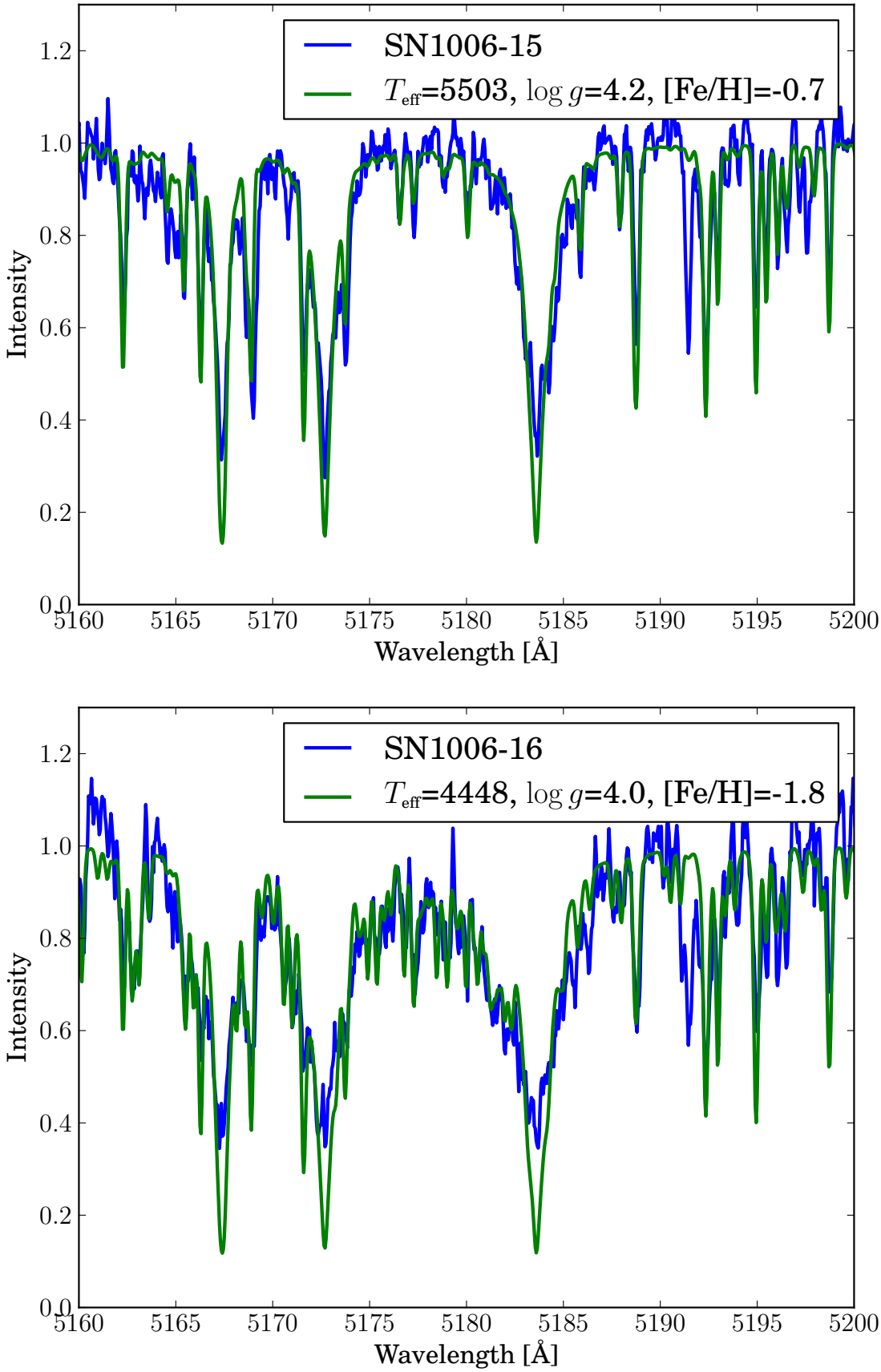

Figure 2.1 Fit of SN 1006 candidate spectra

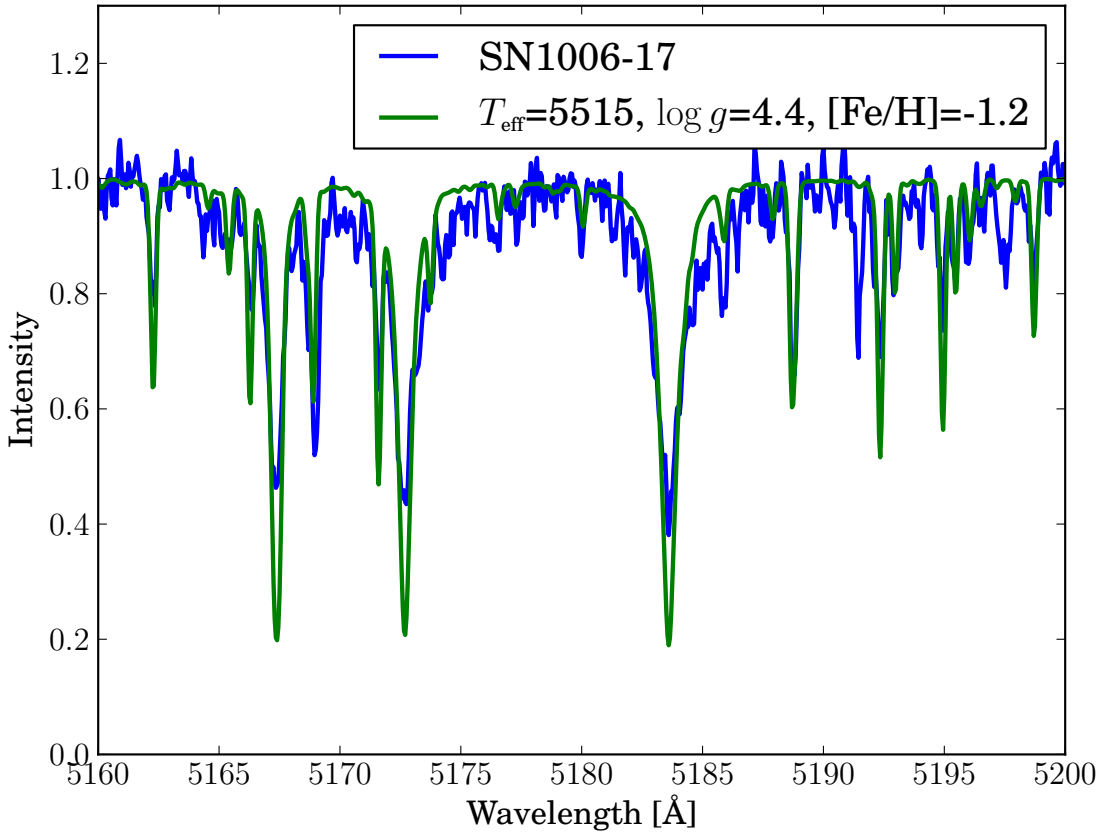

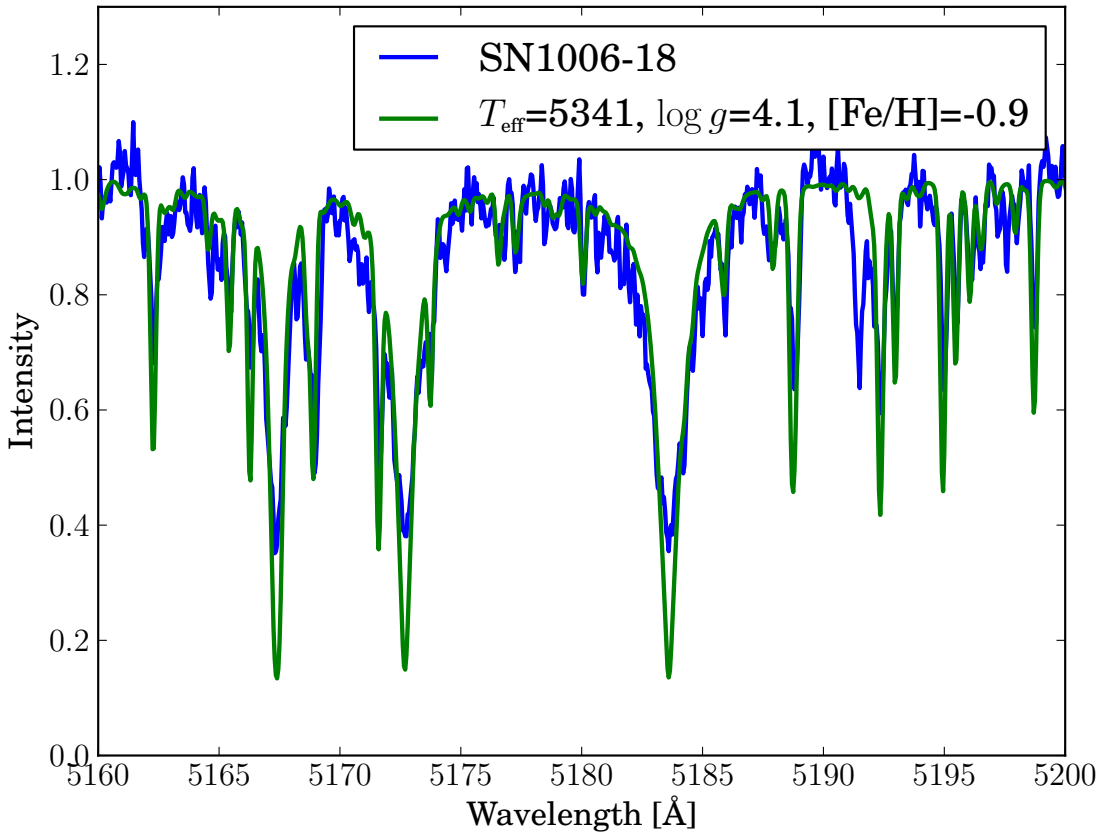

Figure 2.1 Fit of SN 1006 candidate spectra

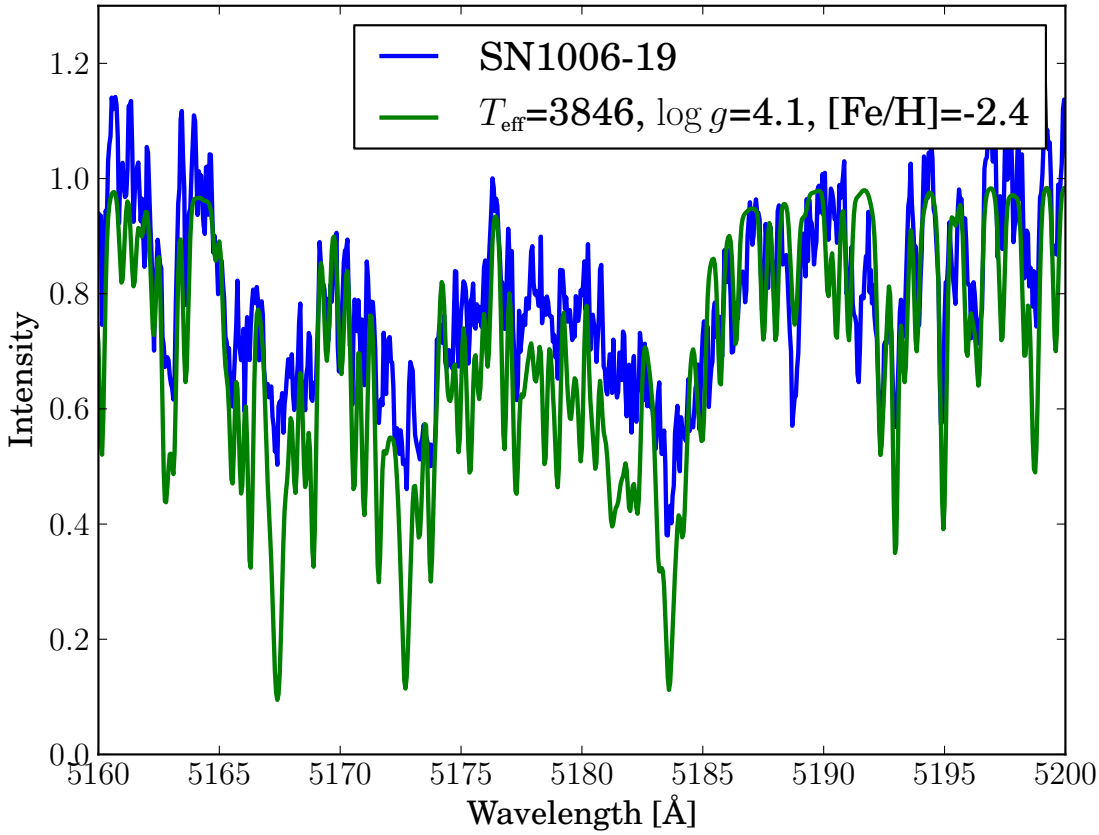

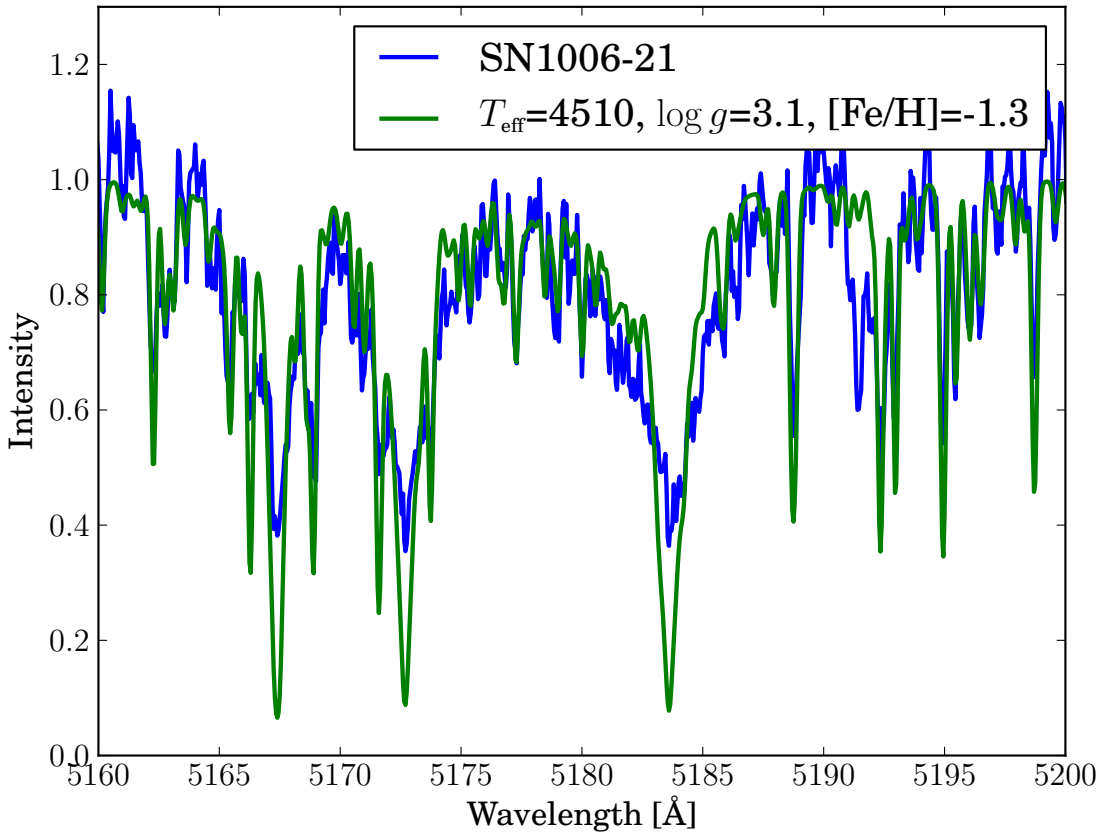

Figure 2.1 Fit of SN 1006 candidate spectra

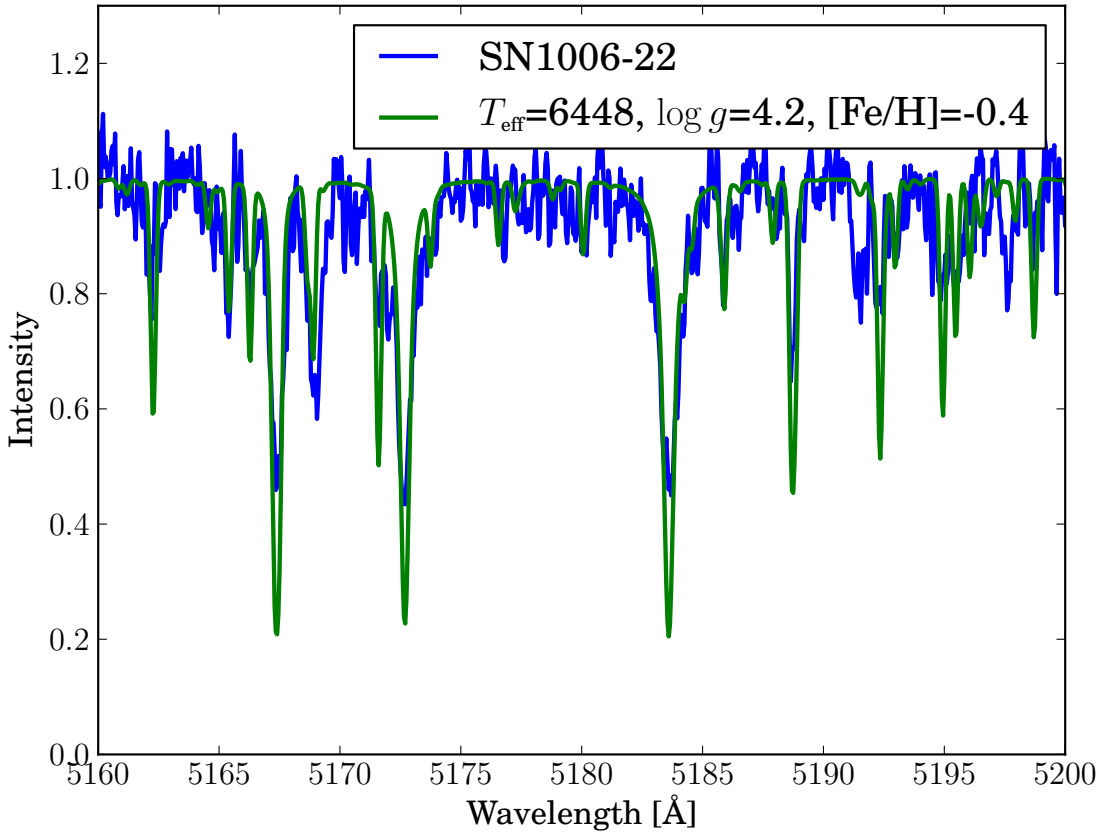

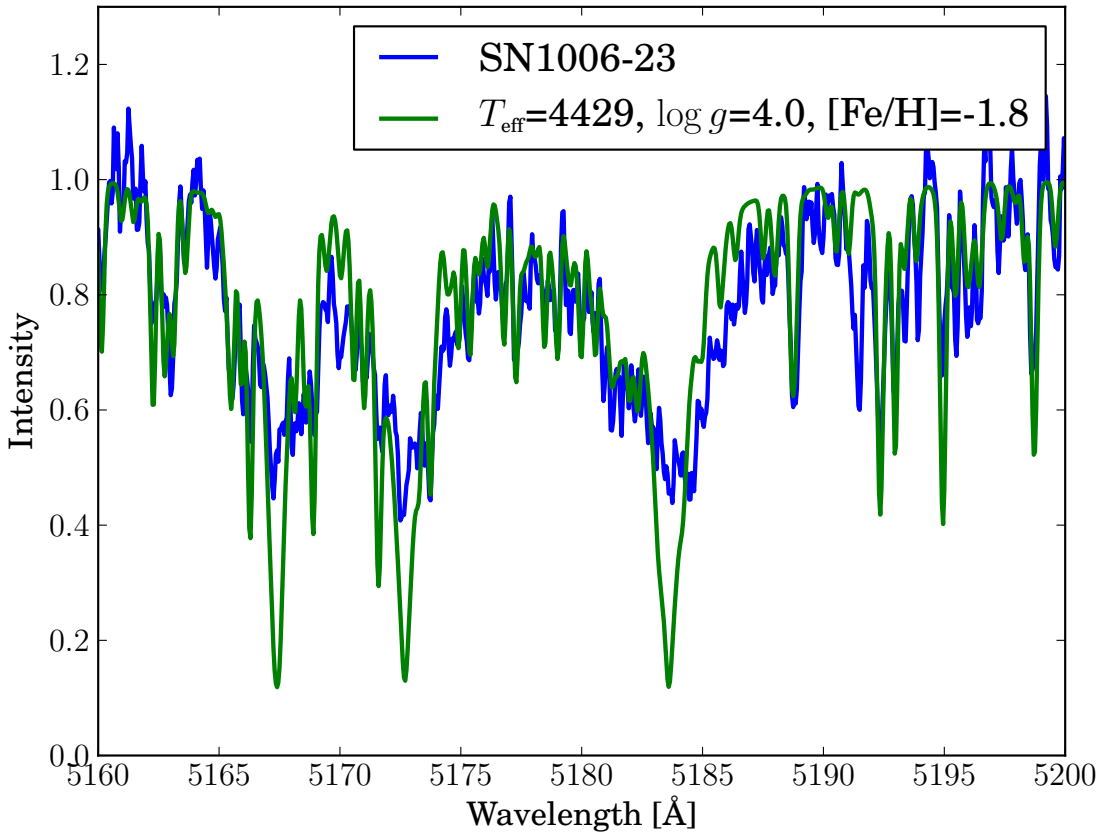

Figure 2.1 Fit of SN 1006 candidate spectra

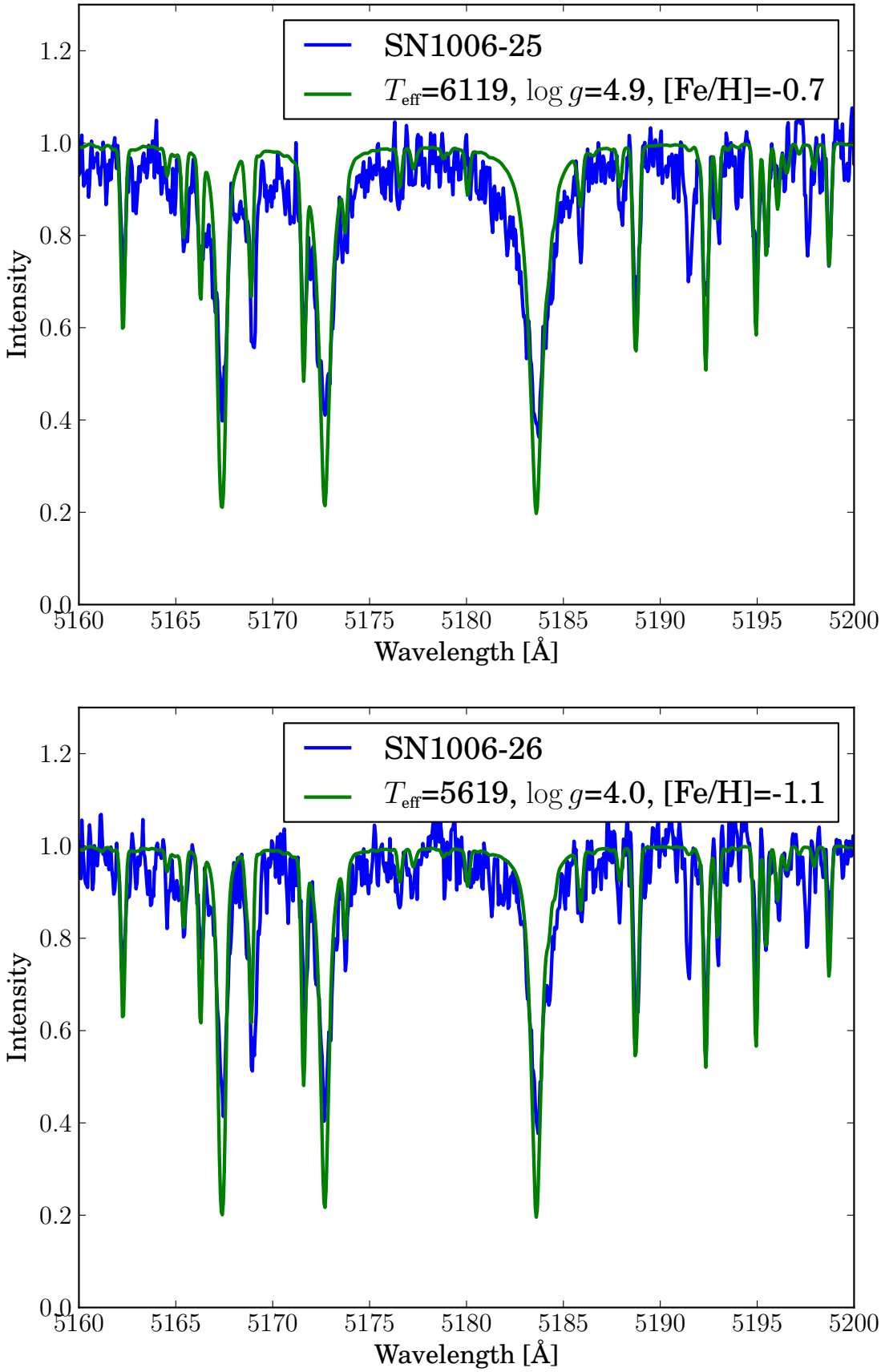

Figure 2.1 Fit of SN 1006 candidate spectra

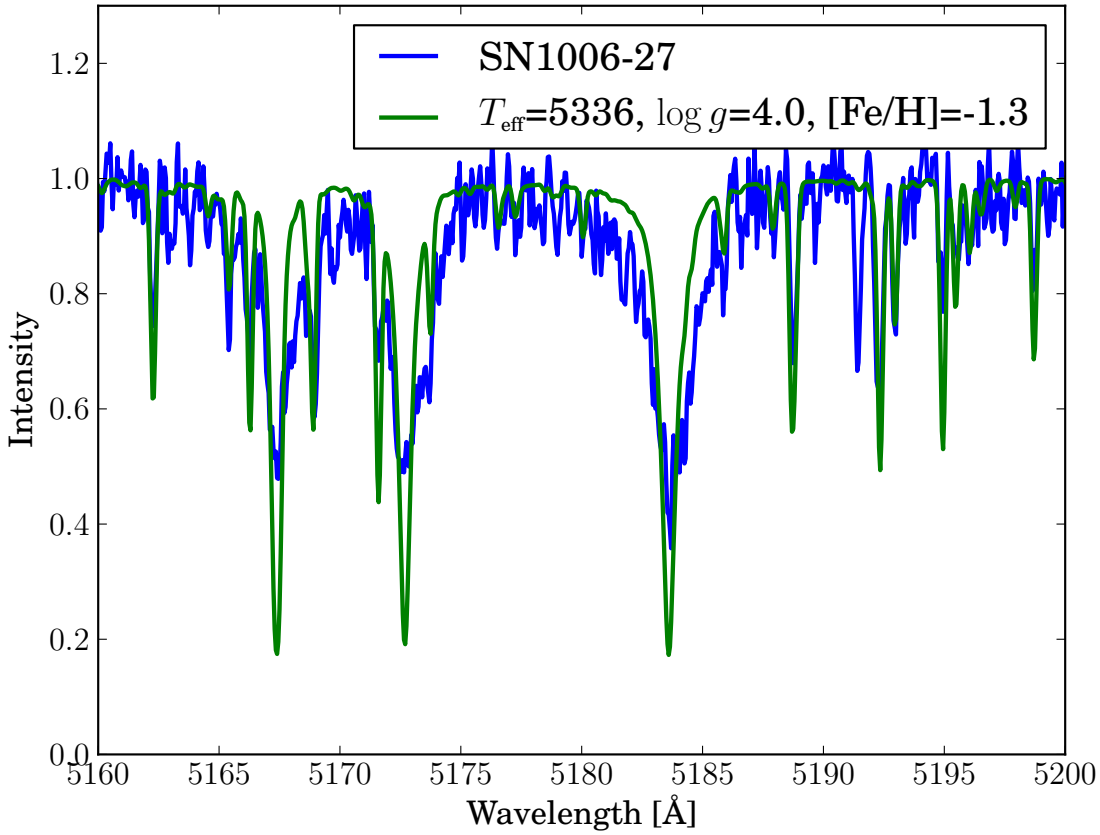

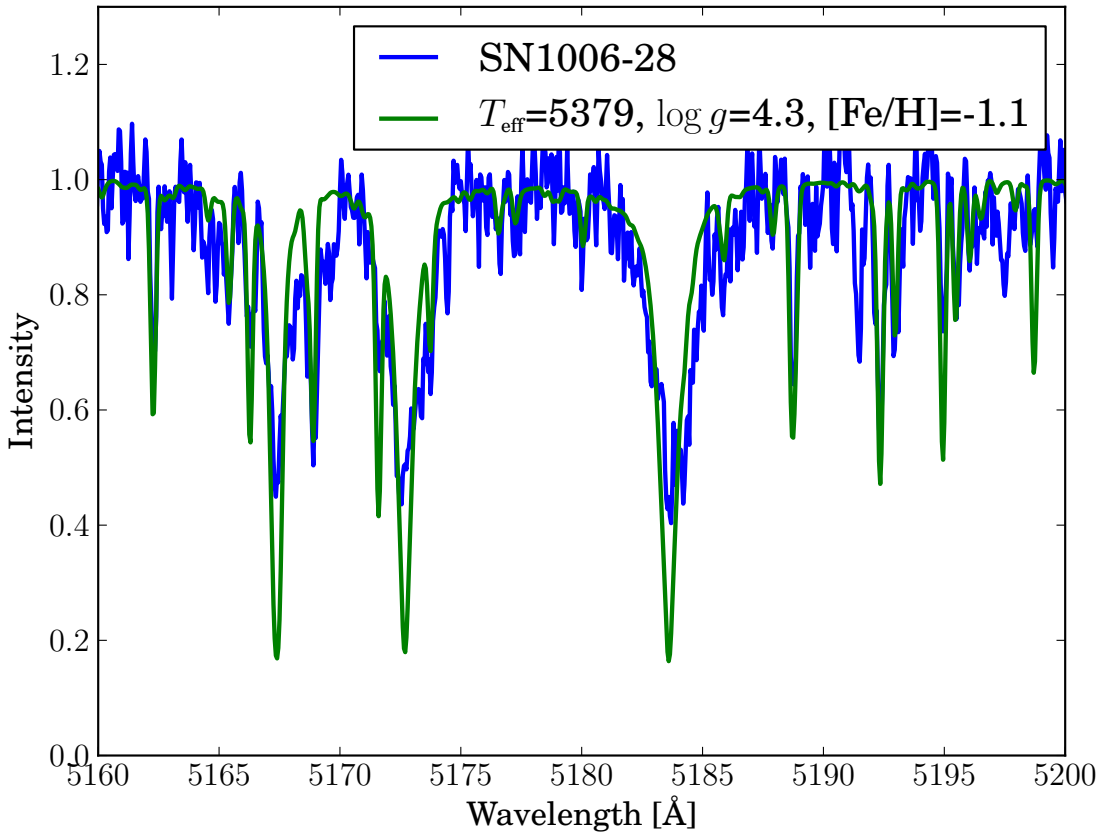

Figure 2.1 Fit of SN 1006 candidate spectra

Bibliography

Barber, C. B., Dobkin, D. P., & Huhdanpaa, H. 1996, ACM TRANSACTIONS ON MATHEMATICAL SOFTWARE, 22, 469

Bertin, E., & Arnouts, S. 1996, A&AS, 117, 393 (ADS entry)

Casagrande, L., Ramírez, I., Meléndez, J., Bessell, M., & Asplund, M. 2010, A&A, 512, A54+ (ADS entry)

Castelli, F., & Kurucz, R. L. 2003, in IAU Symposium, Vol. 210, Modelling of Stellar Atmospheres, ed. N. Piskunov, W. W. Weiss, & D. F. Gray, 20P–+ (ADS entry)

Goldstein, B. R., & Peng Yoke, H. 1965, AJ, 70, 748 (ADS entry)

Gray, D. F. 1977, ApJ, 211, 198 (ADS entry)

Gustafsson, B., Edvardsson, B., Eriksson, K., Jørgensen, U. G., Nordlund, Å., & Plez, B. 2008, A&A, 486, 951 (ADS entry)

Hamilton, A. J. S., Fesen, R. A., Wu, C.-C., Crenshaw, D. M., & Sarazin, C. L. 1997, ApJ, 481, 838 (ADS entry)

Han, Z. 2008, ApJ, 677, L109 (ADS entry)

Hinkle, K., Wallace, L., Valenti, J., & Harmer, D. 2000, Visible and Near Infrared Atlas of the Arcturus Spectrum 3727-9300 A, ed. Hinkle, K., Wallace, L., Valenti, J., & Harmer, D. (ADS entry)

Kupka, F. G., Ryabchikova, T. A., Piskunov, N. E., Stempels, H. C., & Weiss, W. W. 2000, Baltic Astronomy, 9, 590 (ADS entry)

Kurucz, R., & Bell, B. 1995, Atomic Line Data (R.L. Kurucz and B. Bell) Kurucz CD-ROM No. 23. Cambridge, Mass.: Smithsonian Astrophysical Observatory, 1995., 23 (ADS entry)

Kurucz, R. L., Furenlid, I., Brault, J., & Testerman, L. 1984, Solar flux atlas from 296 to 1300 nm, ed. Kurucz, R. L., Furenlid, I., Brault, J., & Testerman, L. (ADS entry)

Maeda, K., Taubenberger, S., Sollerman, J., Mazzali, P. A., Leloudas, G., Nomoto, K., & Motohara, K. 2010, ApJ, 708, 1703 (ADS entry)

Marietta, E., Burrows, A., & Fryxell, B. 2000, ApJS, 128, 615 (ADS entry)

Robin, A. C., Reylé, C., Derrière, S., & Picaud, S. 2003, A&A, 409, 523 (ADS entry)

Schweizer, F., & Middleditch, J. 1980, ApJ, 241, 1039 (ADS entry)

Skrutskie, M. F., et al. 2006, ApJ, 131, 1163 (ADS entry)

Sneden, C. 1973, ApJ, 184, 839 (ADS entry)

Tonry, J., & Davis, M. 1979, AJ, 84, 1511 (ADS entry)

van Dokkum, P. G. 2001, PASP, 113, 1420 (ADS entry)

Winkler, P. F., Gupta, G., & Long, K. S. 2003, ApJ, 585, 324 (ADS entry)

Winkler, P. F., Long, K. S., Hamilton, A. J. S., & Fesen, R. A. 2005, ApJ, 624, 189 (ADS entry)

Wu, C.-C., Crenshaw, D. M., Fesen, R. A., Hamilton, A. J. S., & Sarazin, C. L. 1993, ApJ, 416, 247 (ADS entry)

Wu, C.-C., Leventhal, M., Sarazin, C. L., & Gull, T. R. 1983, ApJ, 269, L5 (ADS entry)